

Electronic Theses and Dissertations, 2004-2019

2012

A Bench Top Study Of The Optimization Of Lvad Cannula Implantation To Reduce Risk Of Cerebral Embolism

William D. Clark
University of Central Florida

 Part of the [Mechanical Engineering Commons](#)
Find similar works at: <https://stars.library.ucf.edu/etd>
University of Central Florida Libraries <http://library.ucf.edu>

This Masters Thesis (Open Access) is brought to you for free and open access by STARS. It has been accepted for inclusion in Electronic Theses and Dissertations, 2004-2019 by an authorized administrator of STARS. For more information, please contact STARS@ucf.edu.

STARS Citation

Clark, William D., "A Bench Top Study Of The Optimization Of Lvad Cannula Implantation To Reduce Risk Of Cerebral Embolism" (2012). *Electronic Theses and Dissertations, 2004-2019*. 2190.
<https://stars.library.ucf.edu/etd/2190>

A BENCH TOP STUDY OF THE OPTIMIZATION OF LVAD CANNULA IMPLANTATION TO
REDUCE RISK OF CEREBRAL EMBOLISM

by

WILLIAM D. CLARK
B.S. University of Central Florida, 2010

A thesis submitted in partial fulfillment of the requirements
for the degree of Master of Science
in the Department of Mechanical, Material, and Aerospace Engineering
in the College of Engineering and Computer Science
at the University of Central Florida
Orlando, Florida

Spring Term
2012

© 2012 William Clark

ABSTRACT

Physical bench top experiments are performed to validate and complement ongoing computational fluid dynamics (CFD) analyses of ventricular assist device (VAD) circulation. VADs are used in patients whose hearts do not function to their maximum potential due advanced stages of heart disease and, consequently, are unable to adequately supply blood to the systemic circulation. VADs are commonly utilized as a bridge-to-transplantation, meaning that they are implanted in patients while waiting for a heart transplant. In such cases of long term utilization of VADs, it has been reported in the literatures that thrombo-embolic cerebral events occur in 14-47% of patients over the period of 6 to 12 months. This is a result of thrombus forming despite the use of anticoagulants and advances in VAD design. Accepting current rates of thrombo-embolisms, the main objective of the project is to identify and propose an optimal surgical cannula implantation orientation aimed at reducing the rate of thrombi reaching the carotid and vertebral arteries and thus reduce the morbidity and mortality rate associated with the long term use of VADs to patients suffering from advanced heart failure. The main focus of the experiment is on the physical aspect using a synthetic anatomically correct model constructed by rapid prototyping of the human aortic arch and surrounding vessels. Three VAD cannula implantation configurations are studied with and without bypass to the left carotid artery or to the Innominate artery with ligation of the branch vessel at its root. A mixture of water and glycerin serves to match blood viscosity measured with a rotating cone-plate viscometer. The Reynolds number in the ascending aorta is matched in the flow model. A closed loop mock circulatory system is then realized. In order to match the Reynolds number in the ascending aorta and LVAD cannula with that of the CFD model, a volumetric flow rate of 2.7 liters per minute is supplied through the synthetic VAD cannula and 0.9 liter per minute is supplied to the ascending aorta. Flow rates are measured using rotary flow meters and a pressure sensor is used to ensure a mean operating pressure of 100 mmHg is maintained. Synthetic acrylic blood

clots are injected at the inlet of the VAD cannula and they are captured and counted at the vertebral and carotid arteries. The sizes of the thrombi simulated are 2, 3.5 and 5 mm which are typical of the range of diameters encountered in practice. Nearly 300 particles are released over 5 separate runs for each diameter, and overall embolization rates as well as individual embolization rates are evaluated along with associated confidence levels. The experimental results show consistency between CFD and experiment. Means comparison of thromboembolization rates predicted by CFD and bench-top results using a Z-score statistic with a 95% confidence level results in 22 of 24 cases being statistically equal. This study provides confidence in the predictive capabilities of the bench-top model as a methodology that can be utilized in upcoming studies utilizing patient-specific aortic bed model.

TABLE OF CONTENTS

LIST OF FIGURES	vi
LIST OF TABLES	viii
NOMENCLATURE.....	ix
CHAPTER ONE: INTRODUCTION.....	1
1.1 Background	1
1.3 Aortic Arch	3
1.4 LVAD.....	5
1.4 Blood	7
1.5 Thrombi.....	8
1.6 Computational Fluid Dynamics	9
1.7 Mean Comparison.....	14
CHAPTER TWO: DESIGN AND PRODUCTION.....	16
2.1 Design and Rapid Prototype of Aortic Arch	16
2.2 Design of Fluid and Matching Reynolds Number.....	23
2.3 Synthetic Blood Clots	26
CHAPTER THREE: BENCH TOP EXPERIMENT	28
3.1 Experimental Setup.....	28
3.2 Data Collection.....	35
CHAPTER FOUR: RESULTS AND DISCUSSION	41
4.1 Comparing Bench Top with CFD Results.....	43
4.2 Bench Top Results	63
CHAPTER FIVE: CONCLUSION.....	73
5.1 Observations	73
5.2 Future Work	73
APPENDIX A: MEAN COMPARISON	75
APPENDIX B: RELATIVE FLOW RATES	77
REFERENCES.....	81

LIST OF FIGURES

Figure 1: Cross section of normal human heart (Taylor 2011).	3
Figure 2: Human aortic arch and branching vessels (Layton, et al. 2006).	5
Figure 3: Debakey LVAD (Osorio, Osorio and Ceballos, et al. 2011).	6
Figure 4: Mesh of CFD aortic arch model.	11
Figure 5: Standard normal distribution.	15
Figure 6: Geometry used for CFD.	17
Figure 7: Converted CFD geometry to be rapid prototyped.	18
Figure 8: Three different LVAD orientations – CAD and actual.	20
Figure 9: LCA bypass connection for shallow configuration.	21
Figure 10: Printed rapid prototype part combined and attached to flow loop.	23
Figure 11: Viscometer with verified viscosity measurement.	25
Figure 12: Particles used in bench top experiment – 2 mm, 3.5 mm and 5 mm.	27
Figure 13: Schematic of bench top experiment.	29
Figure 14: National Instruments terminal block.	30
Figure 15: Pressure transducer attached near descending aorta.	31
Figure 16: Cross section and side view of flow rate sensor.	32
Figure 17: Rapid prototyped injection system introducing particles to flow loop.	33
Figure 18: 3-valve injection system.	33
Figure 19: Three injection entry configurations, from left to right: inside, centered, and outside.	34
Figure 20: Heat exchanger and thermal-hydrometer inside fluid reservoir.	35
Figure 21: PVC T Connection.	37
Figure 22: Particle capture can.	38
Figure 23: Particle separator and measurement device.	39
Figure 24: Camera apparatus for high FPS recordings of particles.	40
Figure 25: 9 different LVAD orientations.	42
Figure 26: Bench top experiment apparatus.	43
Figure 27: Stokes number at various locations in the aortic arch.	46

Figure 28: Intermediate LVAD cannula studied with no bypass.	47
Figure 29: Particle traces for intermediate with no bypass.	55
Figure 30: Particle tracks for perpendicular no bypass.	59
Figure 31: Particle tracks for shallow no bypass.	62
Figure 32: Shallow with LCA bypass and occluded LCA.	64
Figure 33: Particle tracks for perpendicular with LCA bypass.	66
Figure 34: Particle traces for intermediate with LCA bypass.	68
Figure 35: Particle tracks for shallow with LCA bypass.	70

LIST OF TABLES

Table 1: Intermediate No Bypass Centered Injection Configuration Results Compared to CFD.	47
Table 2: Testing criteria for null hypothesis, $\mu = \mu_0$	48
Table 3: Intermediate No Bypass Summarized Results.	50
Table 4: Summary of centered, inside and outside injection configurations.	54
Table 5: Perpendicular with No Bypass Compared to CFD.	56
Table 6: Shallow with No Bypass Compared to CFD.	60
Table 7: Summarized Results for LCA bypass.	63
Table 8: Summary of Results.....	72

NOMENCLATURE

AO	Ascending Aorta
BT	Bench Top
CFD	Computational Fluid Dynamics
DA	Descending Aorta
DAQ	Data Acquisition
LCA	Left Carotid Artery
LSA	Left Subclavian Artery
LVAD	Left Ventricular Assist Device
LVA	Left Vertebral Artery
RCA	Right Carotid Artery
Re	Reynolds Number
RSA	Right Subclavian Artery
RVA	Right Vertebral Artery
St	Stokes Number
VA	Vertebral Arteries

CHAPTER ONE: INTRODUCTION

1.1 Background

Left ventricular assist devices (LVADs) have been accepted as palliative treatment for patients with heart failure awaiting a heart transplant. This is referred to as the bridge-to-transplantation. However, the number of patients requiring heart transplantation is greater than the number of available heart donors, and thus LVADs have also been developed for long term use in patients with advanced stages of heart disease. The survival rate is 50% at one year for patients equipped with LVADs (Davies, et al. 2008, Russo, et al. 2009). Although showing promising results, there are still a variety of complications associated with long term LVAD use, one of which being thromboembolism. Thrombi can form within the LVAD itself or enter the LVAD and then carried to the carotid and vertebral arteries resulting in stroke for the patient.

Previous studies using computational fluid dynamics (CFD) were aimed at reducing the probability of thrombi entering the cerebral arteries by tailoring the outflow cannula on the LVAD (Osorio, Kassab, et al. 2009, Osorio, Osorio and Tran, et al. 2010, Osorio, Osorio and Ceballos, et al. 2011, Argueta-Morales, Tran, et al., Use of Computational Fluid Dynamics (CFD) to Tailor the Surgical Implantation of a Ventricular Assist Device (VAD): A Patient-Specific Approach to Reduce Risk of Stroke 2010). Instead of focusing on the reduction of thrombus formation in LVADs, these studies departed from the premise of accepting current rates of thrombus formation in LVAD-fitted patients and proposed to design an optimal LVAD outflow cannula implantation that would lead to redirection of thrombi away from the cerebral vessels. They investigated the LVAD cannula anastomosis to the aortic arch at various locations, most commonly at some position along the ascending aorta between the aortic root and the take-off of the innominate artery, and at various orientations with respect to the normal of the left lateral wall of

the aorta with the objective of redirecting the thrombi away from cerebral vessels along less problematic vessels such as the descending aorta. These CFD studies demonstrated that within the limitations of the CFD model, in the case of synthetic arch geometries as well as patient-specific geometries, that LVAD implantation configuration is an important factor and should be taken into consideration and that the risk of stroke may be significantly reduced by as much as 50% by tailoring the VAD implantation by a simple surgical maneuver.

The purpose of the work undertaken in this thesis project is to create a physical bench top model replicating the geometry and flow conditions of the CFD models of Osorio et al 2011 in order to experimentally validate the CFD predictions. The ultimate goal is to utilize the bench top model predict the rates at which the synthetic thrombi of various sizes reach carotid and vertebral arteries in the bench top experiments and to statistically compare these predictions with those of the CFD with the aim of establishing the level of consistency between the two sets of experiments.

1.2 The Heart

The heart is a muscle that pumps blood through the circulatory system to perfuse organs and tissues in order to ensure their proper function. The heart is divided into four chambers, two atria and two ventricles, and each of those make up the left and right heart. Oxygenated blood from the lungs enters the right heart which then supplies it to the rest of the body through arterial system and ultimately the capillaries. Deoxygenated blood is returned to the left heart through venous system and then pumped to the lungs to be again oxygenated. The heart pumps blood by period contractions. Since the left heart is responsible for pumping oxygenated blood to the systemic circulation, it is larger than the right heart. The left ventricle has approximately three times the mass of the right ventricle. Therefore, patients that have a weakened left heart due to heart disease have an inadequate amount of

oxygenated blood being pumped to the systemic circulation. Heart failure is a major public health problem affecting over 5 million people in the USA (Lietz, et al. 2009). Orthotropic heart transplantation is the best treatment option for patients with end-stage heart failure; however, the number of patients awaiting heart transplantation far exceeds the number of donor hearts available (Pal, et al. 2009).

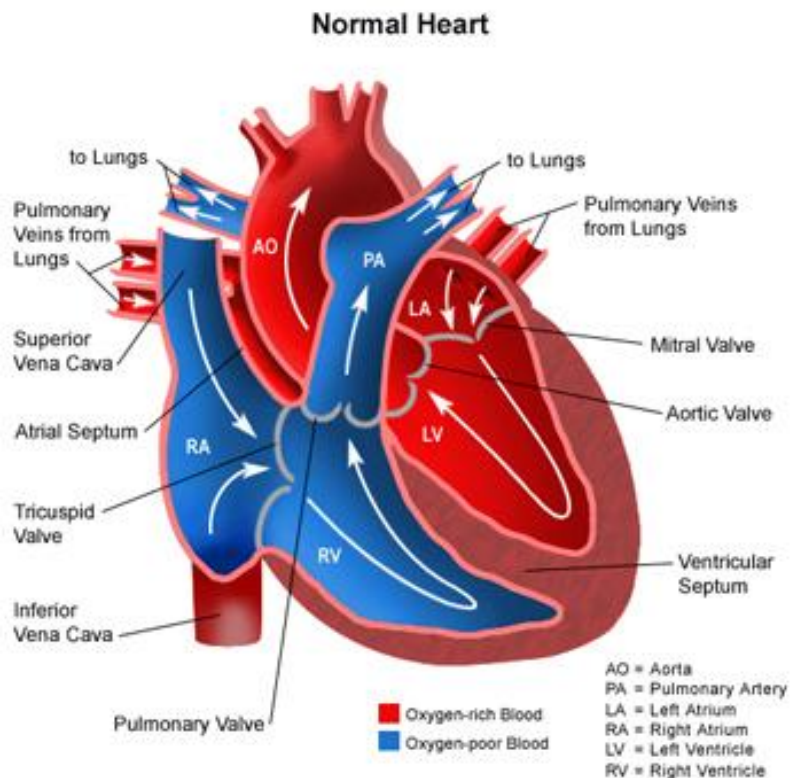


Figure 1: Cross section of normal human heart.

1.3 Aortic Arch

The ascending aorta (AO) is the first and largest artery leaving the heart from the left ventricle and branches off to supply blood to all of the different sections of the body. The most common aortic arch branching pattern in humans consists of three great vessels originating from the arch of the aorta (Layton, et al. 2006). The first of the three great vessels that originate from the aortic arch is the

innominate artery (IA) which branches into three different arteries. These branches are the right carotid artery (RCA), right vertebral artery (RVA) and right subclavian artery (RSA) where the carotid and vertebral arteries supply the brain with blood and the subclavian arteries supply the upper body. Traveling further down the aortic arch, the branch after the innominate artery is the left carotid artery (LCA). The last major branch is the left subclavian artery (LSA) which bifurcates into the left vertebral artery (LVA). The model for the experiment ends at the descending aorta (DA) which supplies blood to the lower extremities. The model studied in this experiment also includes the coronary arteries (CA) that supply the heart itself with blood to ensure its proper function. It is located at the root of the AO and the first vessels to branch off of the aortic arch.

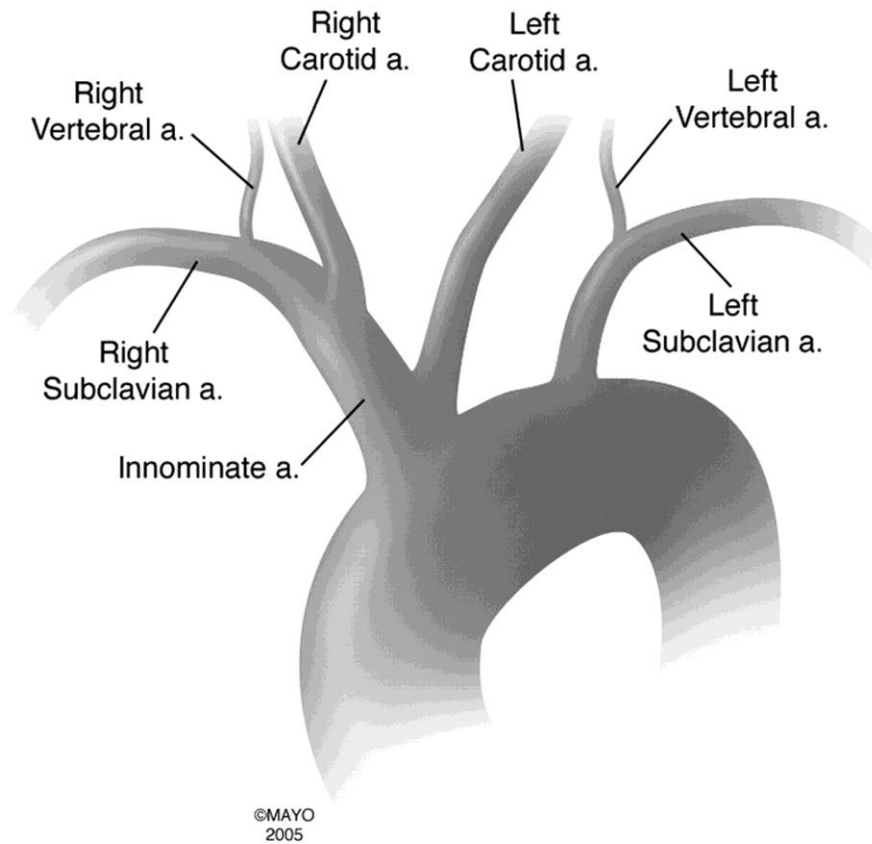


Figure 2: Human aortic arch and branching vessels.

1.4 LVAD

The two main types of LVADs are pulsatile flow and continuous flow pumps. The pulsatile type is designed to match cardiac output (Miller, et al. 2007, Pagani, et al. 2009). In this experiment, The LVAD modeled is a continuous flow axial pump. This specific LVAD is named the DeBakey VAD or HeartAssist5, manufactured by MICROMED Inc. The LVAD with the continuous flow pump significantly reduces pulsatility (John 2008) and in some cases can be designed to eliminate the normal pulsatility (Laufer, et al. 2000) associated with the native circulation. Continuous flow LVADs have shown much promise in terms of durability and superior clinical outcome (Slaughter, et al. 2009). Preservation of organ function

using continuous flow LVADs has been demonstrated in a long term study (Radovancevic, et al. 2007). In patient use, the LVAD is surgically attached to the base of the heart, the apex of the left ventricle in particular, and supplies blood from the left ventricle to the aortic arch. While the heart is still pumping, only a small percentage of blood, if any, is traveling from the left ventricle to the aortic arch while most of the flow is rather supplied through the pump typically to the ascending aortic arch. The LVAD thus takes on a large function of the left side of the heart.

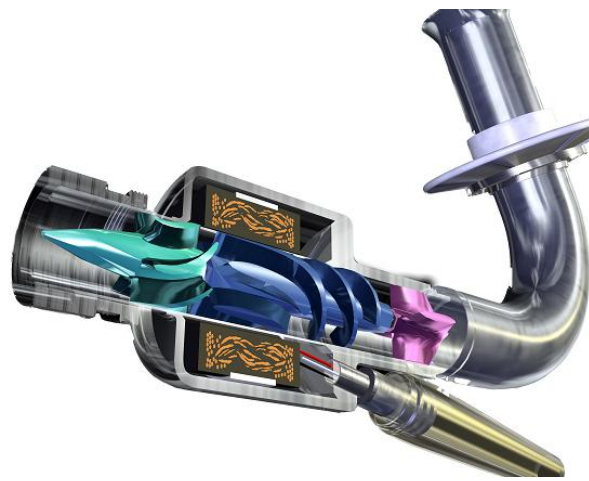


Figure 3: DeBakey LVAD.

At the present time, mechanical circulatory support is the most promising alternative to cardiac transplantation (Goldstein, Oz and Rose 1998). LVADs were typically used as the intermediate step in a heart transplant, keeping the patient alive while they are awaiting a donor heart. This is referred to as the bridge-to-transplantation. Also, LVADs are now being used in long term cases for patients that are terminally ill and patients that were not approved to receive a donor heart. The well-documented imbalance between the number of potential transplant recipients and available donor organs, and the

technological advances in device design and miniaturization has allowed LVADs to become a well-established therapy for adults and children (Slater, et al. 1995).

Survival with LVADs is currently in the range of 50% at 1 year (Davies, et al. 2008, Russo, et al. 2009). The first large-scale, randomized trial that tested long-term support with an LVAD reported a 44% reduction in the risk of stroke or death in patients treated with an LVAD (Lazar, et al. 2004). Furthermore, follow up studies have reported that patients, children or adults, requiring pre-transplantation VAD support have long-term survival similar to that of patients not receiving mechanical circulatory support (Davies, et al. 2008, Russo, et al. 2009). However, there are numerous adverse events that may occur following initiation of circulatory support that can substantially diminish the benefit of this life-saving technology (Frazier and Kirklin 2006). Bleeding, right-sided heart failure, air embolism, and progressive multisystem organ failure are the most common causes of early morbidity and mortality after placement of a LVAD. The most common complications in the late postoperative period are infection, thromboembolism, and failure of the device (Goldstein, Oz and Rose 1998).

1.4 Blood

Blood is the fluid of the circulatory system and is the medium by which substances travel throughout the body. Blood is composed of 40-45% formed elements. Formed elements are red blood cells, white blood cells, and platelets which are responsible for O₂/CO₂ transport, immune response, and blood clot formation, respectively. The remaining 55-60% of blood is plasma. Blood plasma is mostly water by volume and suspends cellular components such as proteins, electrolytes, hormones, and nutrients. Blood is pumped at rate of approximately 4 L/min at rest and 7 L/min during physical activity in a healthy adult. The density of blood is slightly more than water at 1060 kg/m³ due to the increased density of red blood cells. Blood viscosity ranges from 3-6 cP (Waite and Fine 2007)

1.5 Thrombi

The most devastating of the complications of an LVAD is neurologic and is caused by embolization of particulate matter or air into the brain. Particulate matter can come from a thrombus that enters the LVAD from the atrium or ventricle or a thrombus that forms within the LVAD (Frazier and Kirklin 2006, Thoennissen, et al. 2006). A thrombus is a blood clot with a density of approximately 1118 kg/m^3 , calculated based on based on the mass and volume fractions of plasma, red blood cells, white blood cells and platelets in whole blood, utilizing a blood hematocrit of 43% that is within a typical normal physiological range of 39–52% (Osorio, Osorio and Ceballos, et al. 2011). The range of thrombus diameters of interest in this study is 2-5 mm. The formation of thrombi (thrombogenesis) in LVADs is attributed to various mechanisms including platelet activation associated with non-physiological flow patterns such as stagnation and recirculating flows (Bluestein, Schoepfoerster and Dewanjee 1996, May-Newman, et al. 2004, Nobili, et al. 2008). Embolization of any cerebral vessels can cause stroke. Systemic thromboembolization has been reported to occur considerably less often than cerebral (Schmid, et al. 1998).

All LVADs carry a risk for thromboembolism. This risk factor has been addressed, mainly, by improving the device design and attempting adequate anticoagulation. State of the art technology is used to generate engineering designs of LVADs that avoid step changes in lumen size, improperly sized conduits, surface imperfections of $10\mu\text{m}$ or larger, sharp transitions of flow, small radius, right angle bends, multiple cross-sectional flow areas, multiple joints, and surface protrusions; with the ultimate goal of minimizing thrombus deposition. Adequate anticoagulation remains a key issue with the use of LVADs; the need to balance the risk of bleeding with that of thrombosis complicates treatment in patients with LVADs, and the ideal regimen for device-related thrombosis prophylaxis has not been determined. Conventional anticoagulation management includes unfractionated heparin (UFH) in the

post-operative period, oral anticoagulants in the outpatient setting, and adjunctive anti-platelet therapy (Radovancevic, et al. 2009, Sandner, et al. 2008, Meuris, et al. 2007). Despite all these efforts, it has been reported that the incidence of thromboembolic cerebral events ranges from 14% to 47% over a period of 6–12 months (Schmid, et al. 1998, Tsukui, et al. 2007).

1.6 Computational Fluid Dynamics

CFD numerically solves the Navier-Stokes equations in order to resolve the flow field (Osorio, Kassab, et al. 2009, Osorio, Osorio and Tran, et al. 2010, Osorio, Osorio and Ceballos, et al. 2011, Argueta-Morales, Tran, et al., Use of Computational Fluid Dynamics (CFD) to Tailor the Surgical Implantation of a Ventricular Assist Device (VAD): A Patient-Specific Approach to Reduce Risk of Stroke 2010), and the data reported in Osorio (2011) are utilized for comparison with bench top results in this thesis. The Navier-Stokes equations, which are mass and momentum equations while neglecting gravity and other body forces, are provided below:

$$\nabla \cdot \vec{V} = 0 \text{ and } \rho \frac{\partial \vec{V}}{\partial t} + \rho(\vec{V} \cdot \nabla)\vec{V} = -\nabla p + \nabla \cdot \tau \quad (1)$$

Where ρ is the mass density, \vec{V} is the velocity and τ is the viscous stress tensor. CFD was used to a model of a human aortic arch vasculature in order to obtain a flow field for blood traveling through the aortic arch and predict the path of thrombi. The physical bench top model of this report is aimed to validate the results from this CFD analysis. The commercially available CFD software Fluent 6.3 (ANSYS Corp., Canonsburg, PA) (ANSYS 2008) was used to perform the CFD analysis. Within Fluent 6.3, Reynolds averaged Navier-Stokes (RANS) equations were solved to account for turbulence in the model utilizing a finite volume-based pressure-correction algorithm and a second order upwinding scheme for the convective derivative. The k- ω SST two-equation closure model was utilized. The equations and the

values of various closure constants are found in the Fluent user manual (ANSYS 2008) as well as the original paper by Menter (1994) and Wilcox's (2006) book on turbulence modeling in CFD. The k- ω SST model avoids empirical wall functions that are required by the k- ϵ model and has provided accurate solutions in a wide variety of flows including decelerating and accelerating flows, round jets and mixing boundary layers encountered in this study.

The solid model was first constructed using SolidWorks® (Dassault Systèmes S.A., Vélizy, France) from measurements of the diameters of the aortic arch at various locations. The grid was created from the solid geometry using a Fluent meshing software package Gambit. The grid consisted of approximately two million tetrahedral cells which was adequate for grid independence. The y^+ value for the first grid point was less than five to place it within the laminar sub layer and accurately capture the boundary layer. The cells increased in size from the walls of the arteries to the central lumen. These cells represented the fluid volume. The fluid volume was blood which was modeled as an incompressible fluid with a density of 1060 kg/m^3 and a dynamic viscosity of 0.004 Ns/m^2 . Since the LVAD being studied was a continuous flow pump, pulsatility was not accounted for and steady state flow was modeled using the k- ω turbulence model. 5% turbulence intensity was imposed with the flow rate set at 3 L/min at the cannula and 1 L/min at the AO root inlets. Split flow boundary conditions were applied to the outlets with the following percentages of the total flow: coronary arteries 1%, carotid arteries 17%, subclavian arteries 15%, vertebral arteries 5%, and descending aorta 62%.

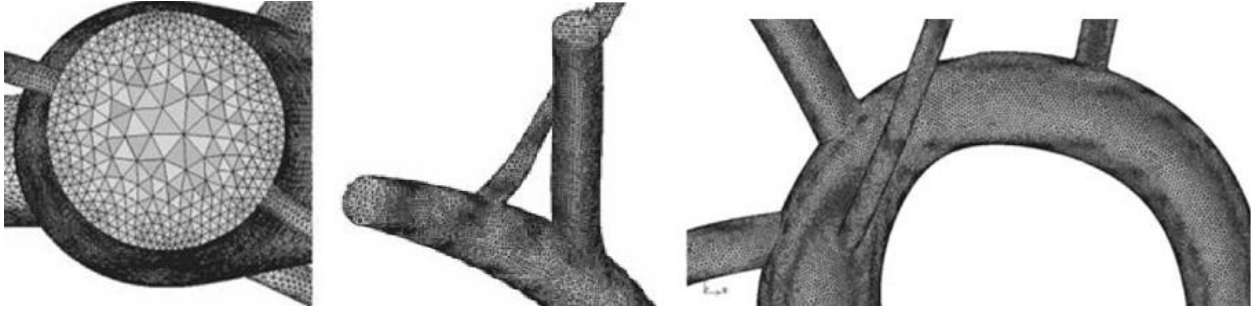


Figure 4: Mesh of CFD aortic arch model.

The thrombi were modeled as spheres in the CFD model with diameters 2-5 mm and density 1118 kg/m^3 . In this approach, the discrete phase (particles/thrombi) is uncoupled from the continuous phase (carrier/blood). In order to analyze the trajectory of the blood clots in the different aortic-arch LVAD models, the trajectories of particles with similar properties to those of thrombi are computed using a mixed Eulerian–Lagrangian approach where thrombi trajectories are predicted using a Lagrangian model in a Newtonian fluid. The thrombi were released from the cannula and enter the flow field of the human aortic arch vasculature. Particles with properties analogous to the blood clots are introduced in the computational domain (at the LVAD conduit inlet plane) and their trajectories are governed by the momentum conservation equation (Newton’s second law of motion) in terms of the particle velocity, \vec{V}_p , and sum of the forces acting on the particle.

$$m_p d \frac{\vec{V}_p}{dt} = \sum \vec{F}_{body} + \sum \vec{F}_{surface} \quad (2)$$

The density of thrombi were calculated based on the mass and volume fractions of plasma, red blood cells, white blood cells and platelets in whole blood, utilizing a blood hematocrit of 43% within a typical normal physiological range of 39–52%. The number of thrombi traveling to an artery was counted and the percentage of thrombi causing embolization to the carotid and vertebral arteries was

calculated. The papers published by this research group and the particle tracking statistics used to compare means can be found in references

The flow field can be displayed after the simulation is converged. An example showing a 2D plane being passed through the geometry at the centerline that describes how the flow behaves with velocity vectors can be seen in Figure 5. In addition to the 2D plane, the figure also shows velocity streamlines that describe the flow field. All three configurations are shown starting with perpendicular at the top, then intermediate in the middle and shallow on the bottom. The maximum average velocity for all three configurations is approximately 6.5 m/s. It is very easy to see the impingement from the LVAD cannula to the contralateral wall of the aortic arch that is later observed by the bench top experiment. The impingement is greatly reduced when the LVAD cannula is shifted down from perpendicular to intermediate to shallow. The impingement zone for the shallow configuration is very weak. A recirculation zone for all three configurations can be visualized. The recirculation zone intensity is directly proportional to the amount of impingement on the contralateral wall of the aortic arch. The velocity streamlines display the Dean vortices, the swirling nature after the bend of the aortic arch, that are generated around curves when the velocity is higher on the outside wall when compared to the inner.

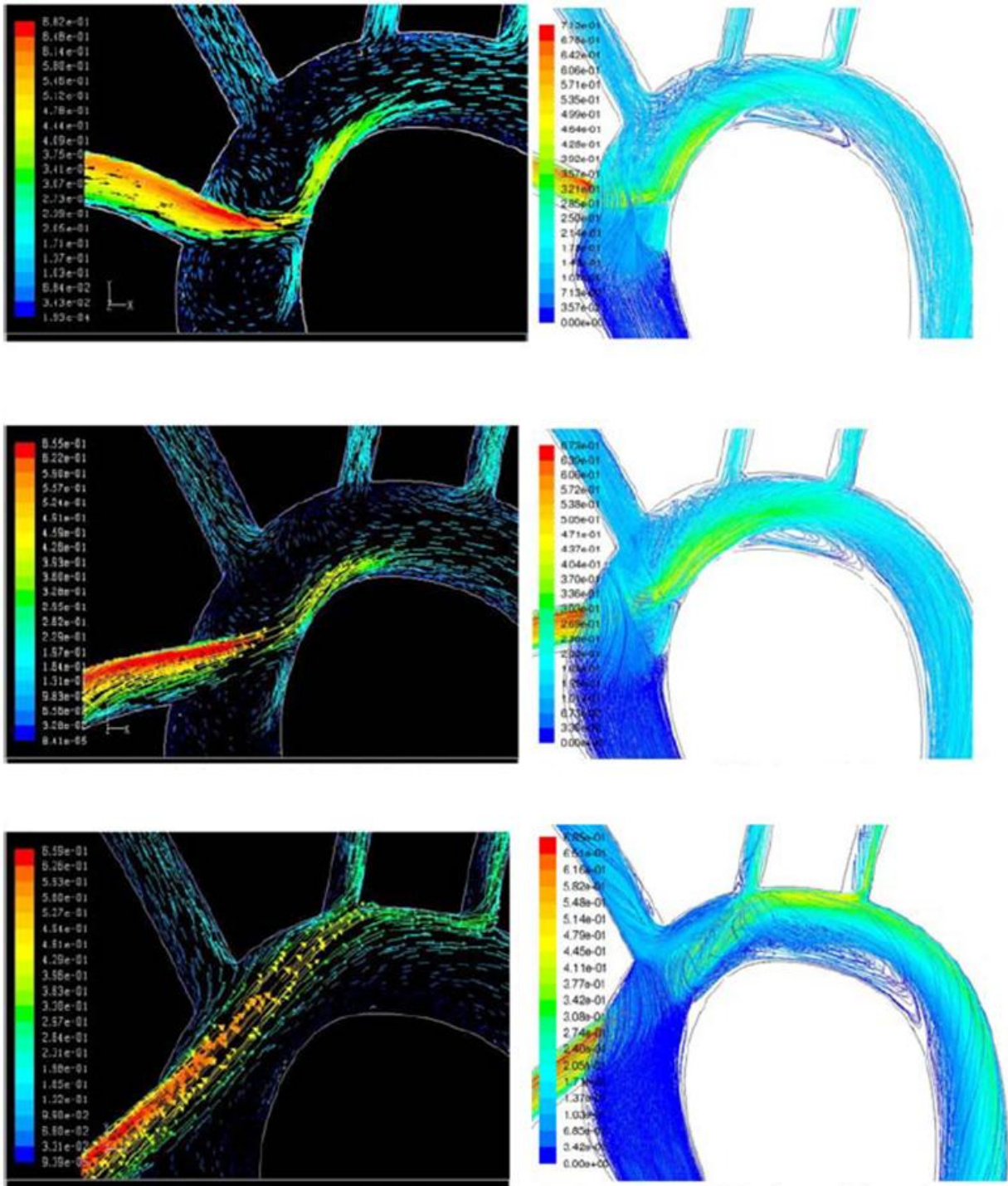


Figure 5: 2D sagittal cutaway with velocity vectors (left) and velocity streamlines (right)

1.7 Mean Comparison

A statistical method utilizing the comparison of two means was employed to determine if the results from the physical bench top model validate those of the CFD analyses. The Z-score was calculated from the probability of thrombi traveling to the carotid and vertebral arteries in the bench top experiment and the CFD:

$$Z = \frac{p_1 - p_2}{p \cdot q \cdot \sqrt{\frac{1}{n_1} - \frac{1}{n_2}}} \quad (3)$$

Where p_1 and p_2 are the probabilities of particles causing embolization from the bench top and CFD models, n_1 and n_2 are the numbers of particles used in each case, p is an overall probability, and $q=1-p$. The Z-score is a standardized statistic that is a measure of the amount of standard deviations away from the mean in a normal distribution. In a normal distribution, 68.2% of the population is one standard deviation away from the mean, 95.4% is two standard deviations away, and 99.7% is three standard deviations away. In this case, the Z-score compares the values from the two different sets of results, and its deviation away from the mean in the normal distribution determines if there is a difference or not between the two compared values. The null hypothesis under consideration was that there is no difference between the results from the bench top experience and the CFD model. The alternative hypothesis was that there is a difference. A Z-score lying within the confidence level, α , results in a rejection of the alternative hypothesis and shows that there is no difference in the two values being compared (Devore 2004).

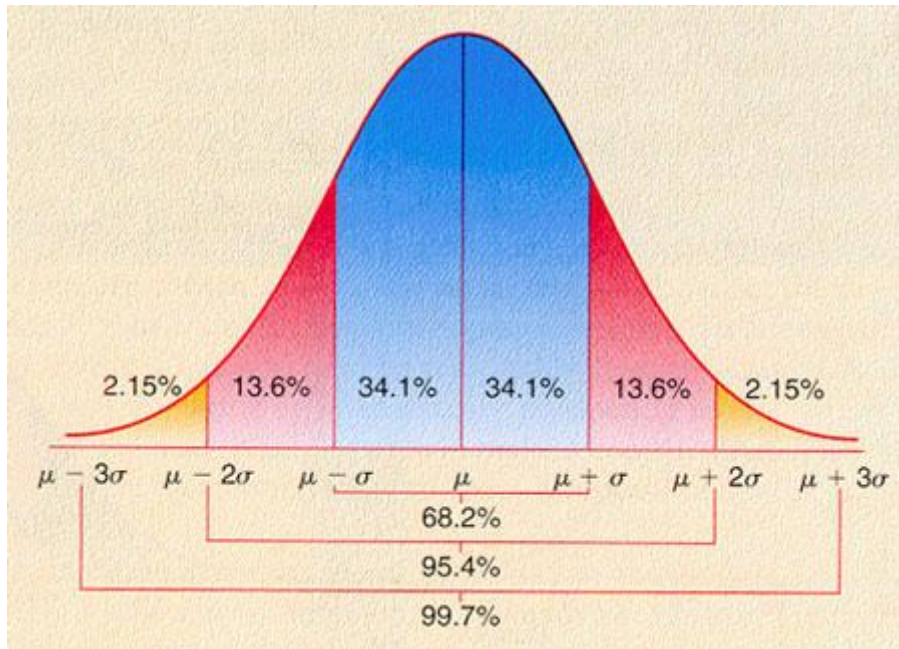


Figure 6: Standard normal distribution.

CHAPTER TWO: DESIGN AND PRODUCTION

The CAD model used for generating the mesh, which is used in CFD software, is utilized as a basis to produce the structure of the final product used for the rapid prototyping of the bench top. All of the inner dimensions are identical, which is imperative when validating results. The construction of the bench top experiment, various modifications, and evolution of the experiment in order to arrive the point where it reliably produced results that could be compared to the CFD are now described.

The computational model is simulated as inner dimensions of the CAD model of the aorta only. This means that any thickness associated to the geometry is neglected. SolidWorks was the CAD package used for drawing the aortic arch. A mesh, which governs the fluid mechanics in the CFD, is then constructed of only the components that will actually touch the fluid. When designing the model for the bench top experiment, a large amount of material must be added to increase the thickness and make the part structurally sound. This is done so the part could be realized with rapid prototyping. The part must also be thick enough that PVC tubing can be fastened to the rapid prototyped model. This is done while maintaining the same inner geometry.

2.1 Design and Rapid Prototype of Aortic Arch

The geometry in its current configuration is a compilation of splines and lofts of various circular cross sections. All of the dimensions, geometry of the aortic arch and surrounding vessels were designed to physiological anatomical specifications. Measurements of the diameter of the aortic arch at selected locations were used to reconstruct a 3D representative solid model of an adult human aortic arch vasculature (Lenter 1990). When adding thickness, nominal tubing dimensions were targets for the final outer diameters.

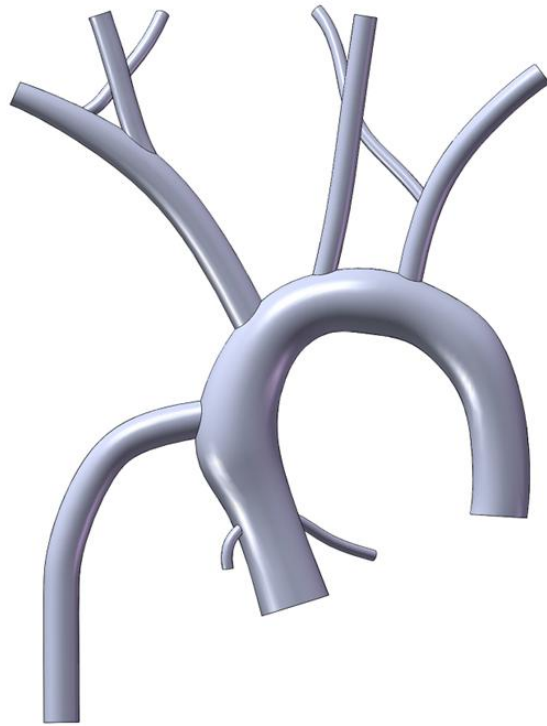


Figure 7: Geometry used for CFD.

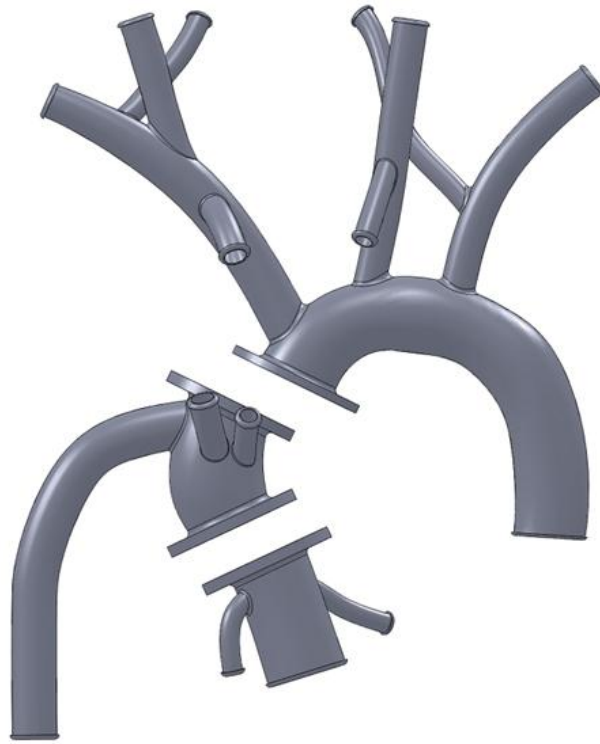


Figure 8: Converted CFD geometry to be rapid prototyped.

There were three separate LVAD configurations studied during CFD analysis. These are referred to as perpendicular, intermediate and shallow cases. The perpendicular LVAD conduit is attached to the aortic arch with an angle of incidence equal to 0 degrees relative to the normal to the right lateral wall of the ascending aorta, see Figure 9. The intermediate LVAD conduit is shifted lower slightly and the angle is decreased by 30 degrees. The shallow LVAD conduit is shifted even lower and the angle is decreased by an additional 30 degrees. It can also be demonstrated that changing the orientation of the LVAD cannula by cutting the outlet of the cannula to the specified angle is straightforward process. One SolidWorks file stores all the configurations and acts as a library for any LVAD orientation or bypass configuration and then a mesh can be generated as described earlier.

Instead of having three different complete rapid prototype models of these configurations, the aortic arch was split into three sections. They are joined by flanges which sandwich rectangular cross section O-rings at convenient locations. The first part and last part are constant. The first part is the base and the ascending aorta. The coronary arteries are also attached to the first part. Three different designs were drawn for the second part corresponding to the three different LVAD cannula configurations. The third part contains the subclavian arteries, carotid arteries, vertebral arteries and descending aorta.

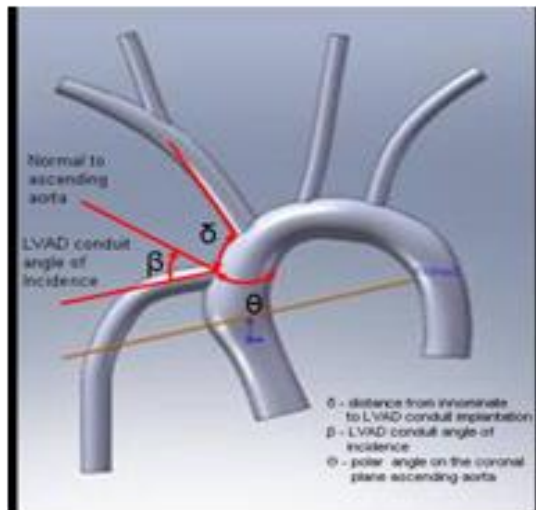


Figure 9: Three different LVAD orientations – CAD and actual.

In addition to three LVAD conduits, there is a bypass that connects the left carotid artery to below where the LVAD conduit is attached on the aortic arch. The LCA is occluded at the base of the

artery and fluid is redirected from the aortic arch through the bypass to the LCA. The bypass is to be studied with the three separate LVAD configurations. There is a different bypass case that will be studied with the three LVAD configurations as well, with similar principles as the first bypass. The connection is between the innominate artery and the aortic arch.

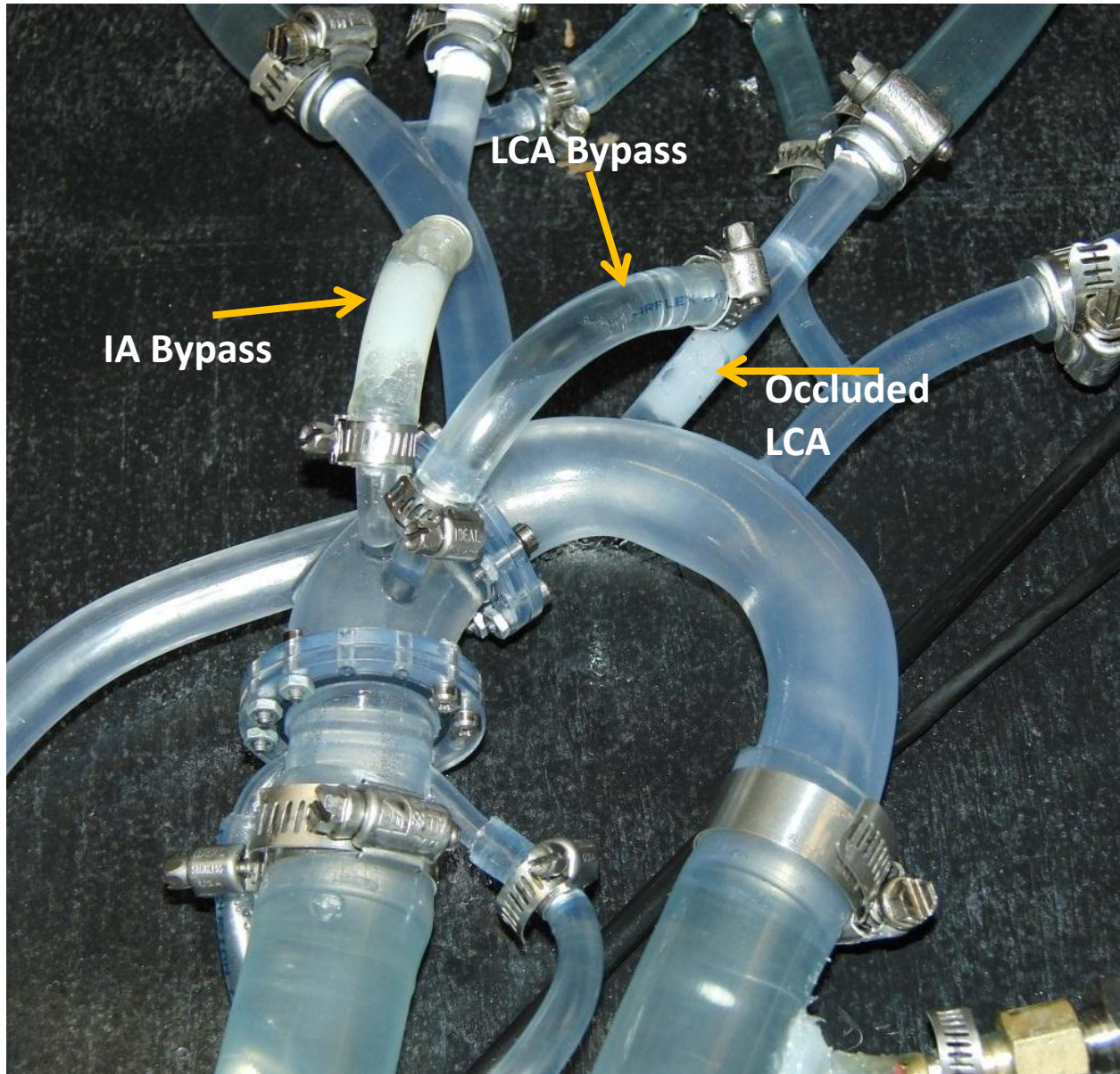


Figure 10: LCA bypass connection for shallow configuration.

Finally, these drawings were sent to Engineering and Manufacturing Services, Inc. in Tampa, FL to be produced via rapid prototyping (RP) process. The material selected was Accura 60. This was chosen for being mostly transparent, which is an important consideration when trying to visualize flow, particle tracking and any possible occlusions. Accura 60 typically is not made to be the medium of fluid transport, so a clear coat of automotive paint was added as a sealant. The sealant smoothed out the rough cloudy surface and also enhanced the transparency. The machine used to produce the part prints in slices and is printed 1/100 of an inch at a time with high resolution so that the RP slice layers form a seamless surface of the finished product.



Figure 11: Printed rapid prototype part combined and attached to flow loop.

2.2 Design of Fluid and Matching Reynolds Number

Water and glycerin were mixed to simulate the density and viscosity of blood. The viscosity of water and glycerin are 0.862 cP and 1294 cP respectively at room temperature. The density of water and glycerin are 1000 kg/m^3 and 1260 kg/m^3 respectively. There is a significant difference in the order of magnitude of the two fluid viscosities. On the other hand, the density disparity is not large at all. When mixing two fluids together, the new density is calculated by a simple sum based on the weights of the fluid chosen for the mixture. For the fluid that is simulating blood's properties, water consists of 60% of the mixture and the last 40% is from glycerin. When mixing and then trying to find the viscosity the

Refutas blending equation can be used to obtain the effective mixture viscosity. The Refutas equation is an empirical relation that requires the input of the viscosities of two fluids in centistokes and produces a mixture viscosity in centistokes based on a weighted average, as shown below.

$$VBI = 14.534 * \ln(\ln(v + 0.8)) + 10.975 \quad (4)$$

$$VB_{Mixture} = W_1 * VBI_1 + W_2 * VBI_2 \quad (5)$$

$$v_{Mixture} = e^{\frac{VB_{Mixture}^{-10.975}}{14.534}} - 0.8 \quad (6)$$

VBI represents the Viscosity Blend Index, where there will be a VBI for each fluid. Then to comprise the Viscosity Blend Mixture, each VBI calculated is multiplied by the percent weight, W, for each fluid. VB Mixture is then used to find the actual viscosity of the mixture. The output of the mixed viscosity is then converted from centistokes to centipoise. The ratio of the mixture was chosen experimentally such that it was easy to measure and also close to the desired viscosity.

The final viscosity of the 60% water - 40% glycerin mixture is 3.801 cP which is approximately viscosity of blood. The equation was verified by a DV-III cone-plate viscometer from Brookfield Engineering. At any temperature, the Refutas equation values match the experimental values provided by the viscometer. While this is a significant validation, the density of the bloods simulation mixture is 1104 kg/m³. The density of blood is 1060 kg/m³, which results in a 4% difference in the density of the mixture and blood.



Figure 12: Viscometer with verified viscosity measurement.

When considering the difference in density, the underlying scaling parameter for the flow loop to match the CFD is that the Reynolds number (Re) that is to be held constant. The Reynolds number is directly proportional to density. While keeping the Reynolds number constant and using the measured density and viscosity of the mixture, the only unknown is velocity. Knowing this, Re can be calculated at

the inlets and then used to calculate the new velocity because of the change in density between the mixtures. The velocity change at the LVAD cannula is 9%. After finding the new velocity at the cannula and ascending aorta, the new inlet volumetric flow rates can be found. The sum of these flow rates are then divided by percentages based on the flow distribution to the outlets. The flow percentages never change between the CFD and the bench top experiment. The only changes made between the bench top and CFD is the volumetric flow at the inlets, while holding the Re constant. These calculations are presented in APPENDIX B: RELATIVE FLOW RATES.

2.3 Synthetic Blood Clots

Thrombi are simulated in the CFD as perfect spheres. This is also the case for the bench top experiment. There is a small disparity in density for the bench top since the value imposed into the CFD is the actual density of thrombi which is 1118 kg/m^3 . The closest density of any common materials was that of acrylic which is approximately 1210 kg/m^3 . There is a 7.6% difference in the densities of the particles studied. While there is a difference in density, it is required that the density of acrylic is greater than the fluid used to represent blood. The diameters of the blood clots simulated in the bench top are 2, 3.5 and 5 mm which are typical of the range of diameters encountered in physiological thrombi.

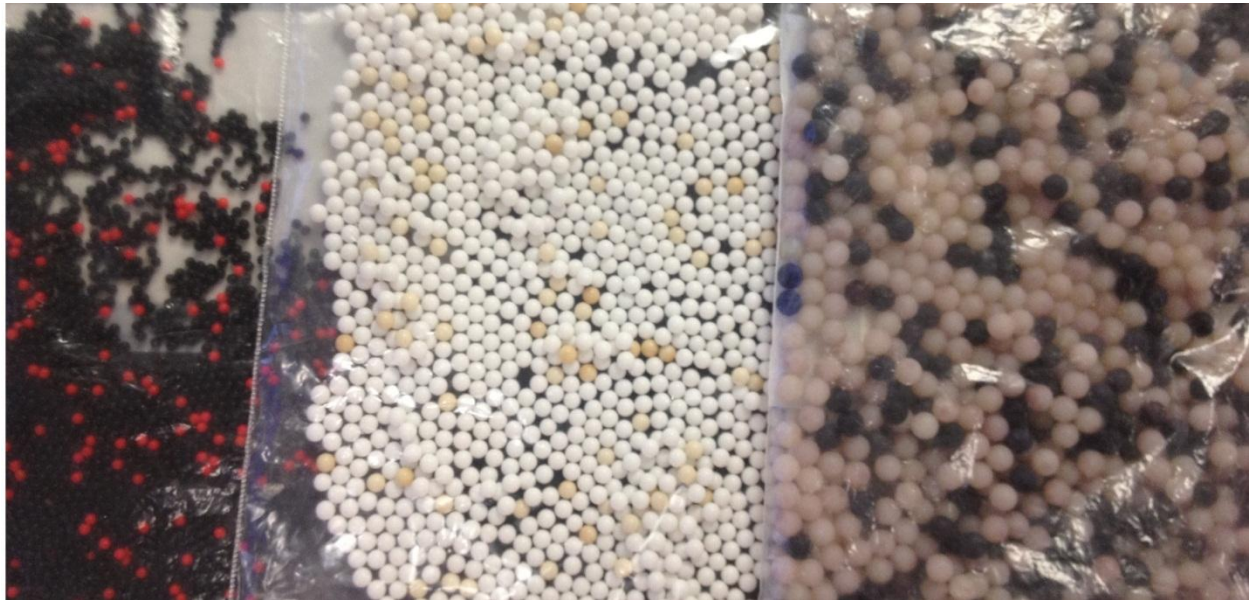


Figure 13: Particles used in bench top experiment – 2 mm, 3.5 mm and 5 mm.

CHAPTER THREE: BENCH TOP EXPERIMENT

The bench top experiment is a closed flow loop of a simplified version of the circulatory system. There are two inlets and seven outlets. Over 100 feet of PVC tubing was used to construct the flow loop. The tubing is also fastened to the rapid prototyped model of the aortic arch and cannula. Physiological flow rates and pressures are achieved by adjusting valves. Neither pressure nor flow rates are geometry driven and is all imposed. Particles are then injected into the flow field with the different LVAD cannula configurations and then captured, sorted and counted.

3.1 Experimental Setup

A schematic was designed encompassing all aspects of the bench top model. The direction of flow can be seen as well as the location of tubing and valves. The schematic shows the reservoir which supplies the synthetic blood to the continuous flow axial centrifugal pump. The pump is attached to an inlet manifold which supplies flow to the system and also has a bypass that redirects flow back to the tank to either help adjust pressure or any flow additional to the 3.6 LPM that is being supplied to the circulatory system.

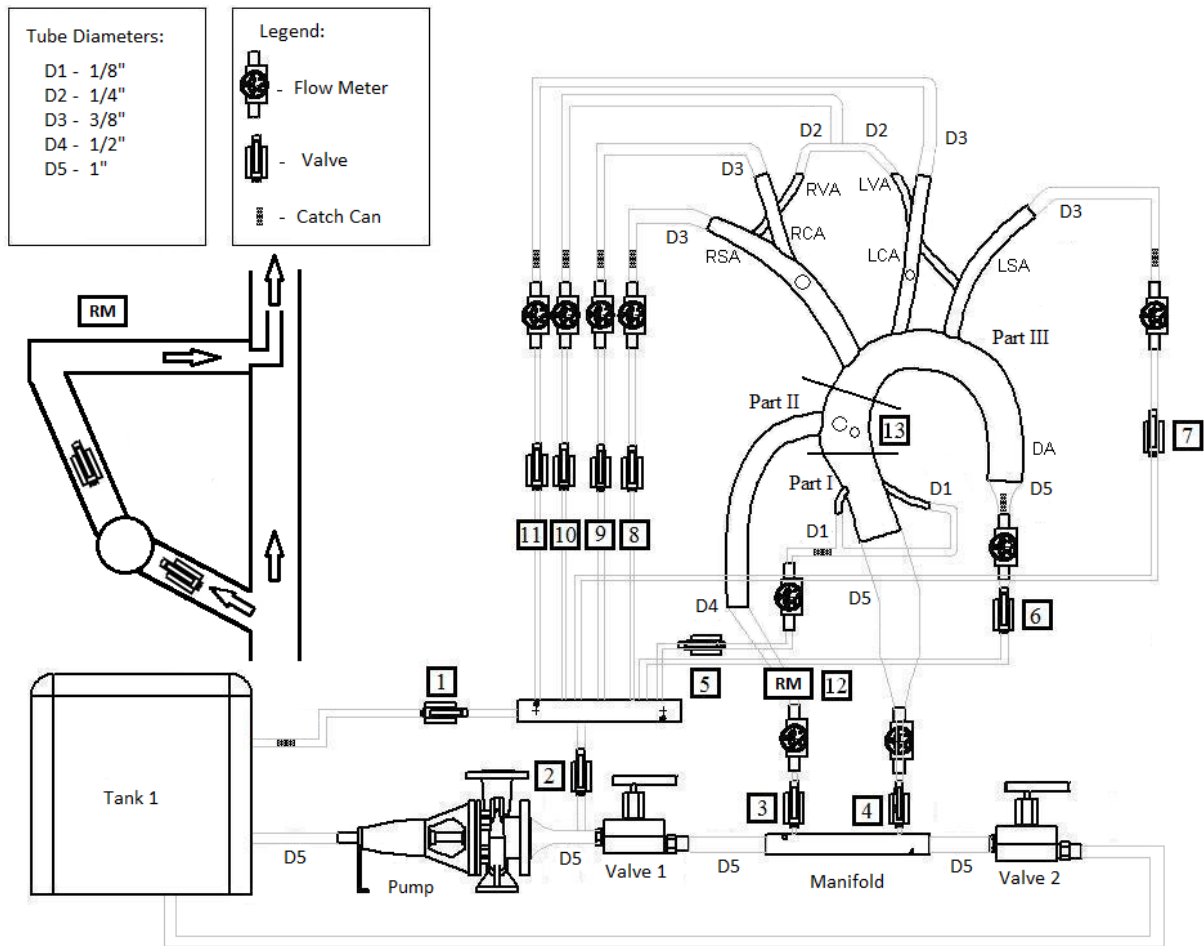


Figure 14: Schematic of bench top experiment.

The location of the flow rate sensors, pressure transducer, particle injection system, rapid prototyped aortic arch, and particle capture cans are shown in the schematic. It also shows an enlarged image of the injection system.

The schematic does not show the data acquisition (DAQ) system that consists of two National Instruments PCI cards which are inserted into the motherboard of the computer. These cards communicate with two separate terminal blocks by receiving information from the pins between the

cables that connect them and the corresponding location of the pins on the DAQ cards. The terminal blocks receive the signal from the flow sensors and the pressure transducer. The pressure transducer only outputs a voltage signal which is easily read by an analog channel in the terminal block. The flow rate sensors are read by counter channels in the terminal block. Counters do a Fast Fourier transform based on the square voltage waveform that is output from the flow rate sensors. The terminal block provides a 5 volt power source that taps into the computer power supply. The flow rate sensors also require 5 volts to be powered. Using this voltage in parallel by the aid of a bus bar, all flow rate sensors are powered. There are 47 wires in total connected to the two terminal blocks. All of these signals are displayed with a National Instruments software package called LabView.



Figure 15: National Instruments terminal block.

The pressure transducer is attached near the descending aorta. Since the flow is steady, the pressure desired is the average of diastolic and systolic pressure. The average pressure is 100 mmHg. A

U-tube manometer was used to calibrate the pressure transducer. Ten readings were taken to determine that the fit was linear. The pressure transducer outputs a voltage and that is then related to a pressure. The maximum pressure the sensor can read is 15 psi.



Figure 16: Pressure transducer attached near descending aorta.

Flow rate sensors are located at all of the inlets and outlets of the bench top. These sensors output a frequency which is related to a volumetric flow rate by a linear fit supplied by the manufacturer. This was also verified by comparing the volume read by the sensor versus the volume supplied. 8 of the 9 flow rate sensors read between 0.1 and 2.5 LPM. The 9th flow rate sensor, located at the cannula, reads from 0.8 to 7.6 LPM. The accuracy of the sensors is $\pm 2\%$. The flow rate sensors are turbine style, a small propeller spins in line with the direction of the flow. A pull-up resistor is required for the sensors to supply a reading. The resistance, 5k Ohms, must be placed between the output line and the power supply. The square wave that is output by the sensor is 'pulled down' there is a voltage difference that was created by the propeller spinning. Fluxes are also measured to assure continuity is held throughout the experiment.

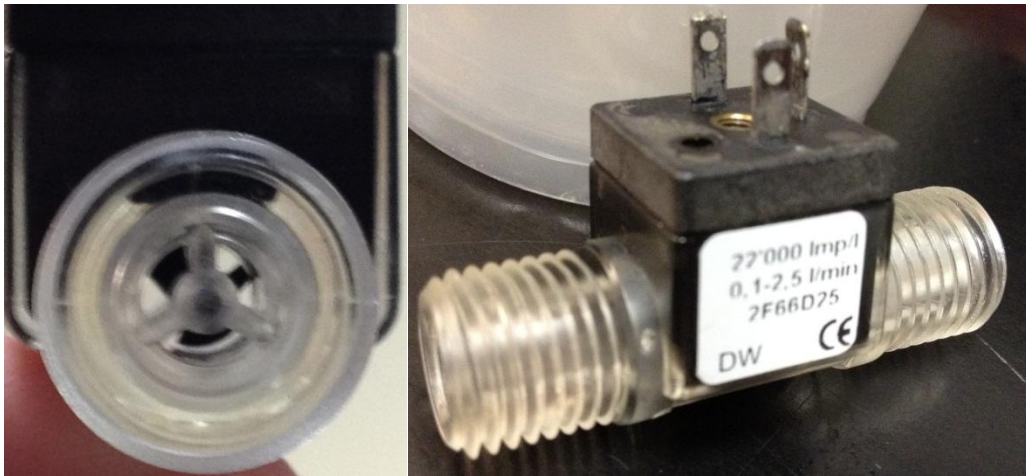


Figure 17: Cross section and side view of flow rate sensor.

Flow rates are controlled by adjusting valves to either increase or decrease flow to a specific vessel. All final flow rates match physiological values. This is an iterative process, when one valve is adjusted the rest of the flow rates are altered because of a change in back pressure. The strategy is to slightly overshoot the flow rates at the inlets and then adjust the valves at the outlet. The small pressure change from these adjustments will correct the flow rates at the inlets. This ensures that all of the flow rates match the physiological values. For continuity, the highest flow rate outlet is left 100% open and all the remaining flow passes through here.

Once all of the physiological flow rates are set, particles are introduced to the flow loop to simulate the blood clots. A flow redirection was utilized to accomplish this. A Y-split was added to the tubing connected to the LVAD cannula. A custom rapid prototyped part consisting of a cylinder inside of a cylinder was then attached so the flow that was separated can be rejoined to the cannula.



Figure 18: Rapid prototyped injection system introducing particles to flow loop.

Three valves are used to introduce and then control the rate at which particles are allowed into the flow loop. Two of the three valves are in-line with the flow and these two valves control the flow rate through the Y-split. The third valve is placed perpendicular to and in-between the other two valves. Then the valve is rejoined with a barbed T connection. With this configuration, flow can be stopped to the Y-split and particles can be introduced.



Figure 19: 3-valve injection system.

The part that introduces the particles into the flow field was also made by rapid prototyping. It was designed to be interchangeable, by flanges, with three different configurations. This was done to best replicate the way particles are released in the CFD. There is a configuration that is on the inside wall, outside wall and the center of the tube.



Figure 20: Three injection entry configurations, from left to right: inside, centered, and outside.

When the flow loop is in operation, it is important to maintain a constant viscosity. The pump is constantly generating heat while it is running, and this heat is transferred to the flow loop fluid which increases the temperature in the tank. For example, the temperature increase for thirty minutes of use was measured to be 30° F which significantly affects the viscosity of the flow loop fluid. A heat exchanger was added to the tank that was connected to a sink faucet to maintain a relatively constant temperature of 76° F during operation. The temperature of the fluid from the sink was 64° F. After the heat exchanger was added the temperature difference of the fluid in the tank after thirty minutes was only 5° F and the change in viscosity is acceptable. With the 5° F temperature difference, the actual change in final viscosity of the mixture changes by 0.079 cP which is only a 2.1% change in viscosity.

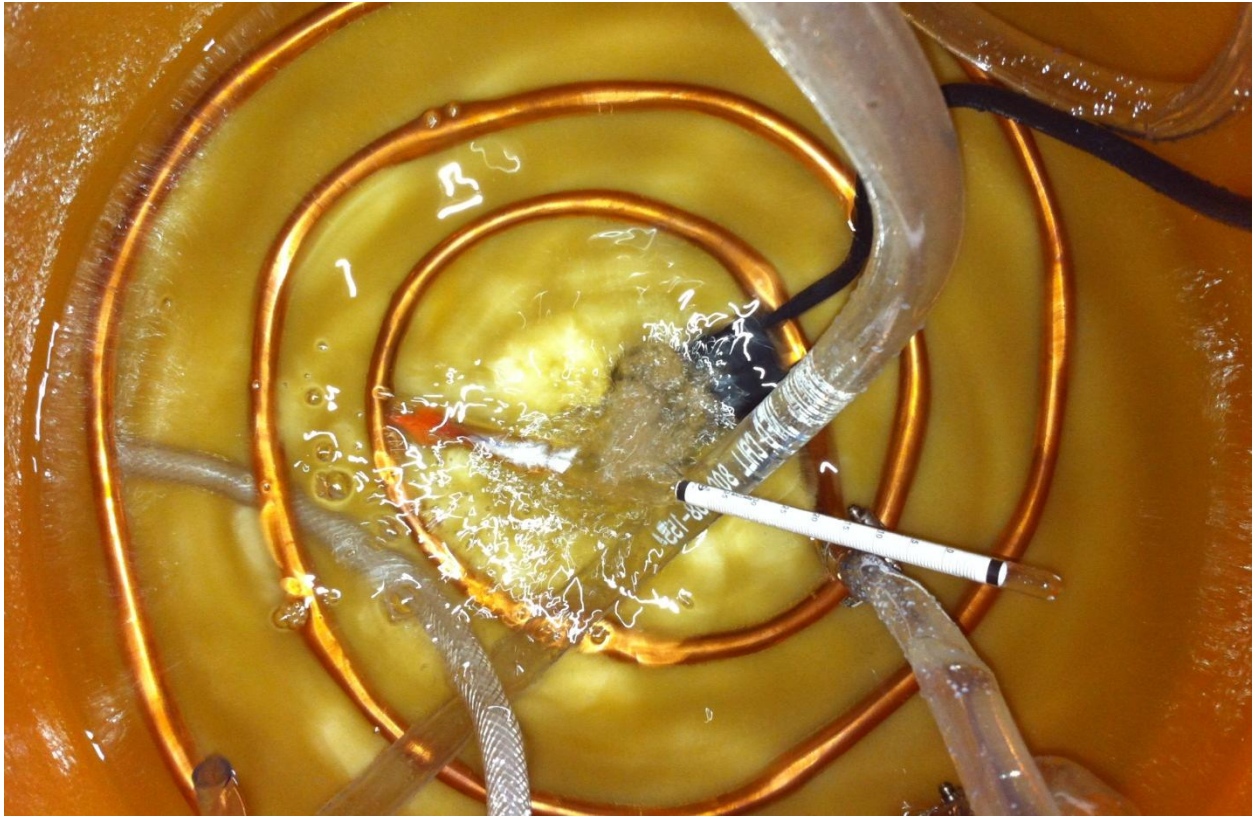


Figure 21: Heat exchanger and thermal-hydrometer inside fluid reservoir.

In addition to monitoring the temperature in the reservoir, the specific gravity was monitored before each test to ensure that a significant amount of water did not evaporate. The mixture of glycerin and water is immiscible and when at rest over time the fluids will separate again. The heavier fluid, glycerin, will sink to the tank bottom, while water remains on top further enhancing the evaporation. To enhance the mixing process a small pump is positioned inside the reservoir and circulates the fluid.

3.2 Data Collection

A series of 2, 3.5 and 5 mm particles were released in sets of 300 particles per test run, and all test runs were carried out for one size at a time. The particles were released in a manner such that there

was no interaction with any other particles. This was a very slow process and was completely controlled by the amount of flow allowed through the Y-split to force particles into the system.

After the particles have reached their destination, they are redirected and then stored in particle capture cans that can be dis-assembled for later counting. The redirection of particles is affected by means of a PVC T-connection. The connection is designed to have one inlet and two outlets. Only one outlet will be used at a given time. The shape of this connection allows flow to be directed either toward the flow sensor or to the particle capture cans where the particles are finally stored. In the direction of the flow to the sensor, the T-connections are lined with a screen mesh that will only let fluid travel through the system and not allow any particles to pass. If particles were to pass through the mesh then the flow sensors could be damaged.

Valves govern flow in the direction of the two outlets and can be alternated, in a binary fashion, when the experiment is ready to have the particles collected or to continue normal operation. During operation, the valve perpendicular to the normal flow is closed and only allows fluid to exit through the outlet attached to the flow rate sensor. When the particles are ready to be extracted, the perpendicular valve is then opened, and this will force the particles into a mesh inside of the particle capture cans.

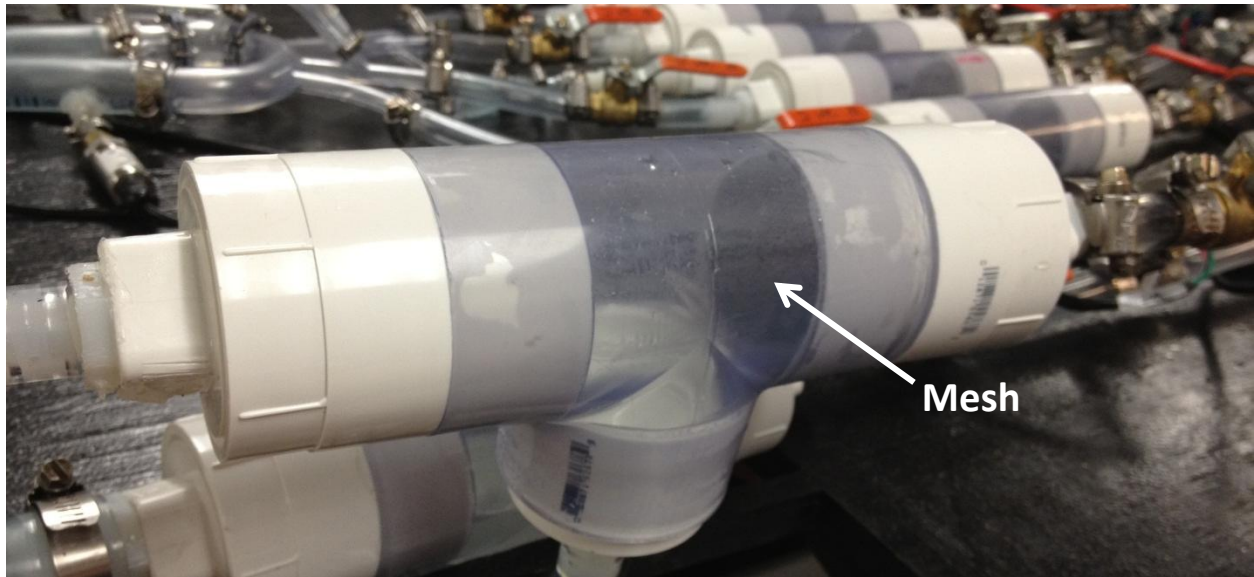


Figure 22: PVC T Connection.

Once flow is redirected, particles are then captured in the particle catch cans. The catch cans consist of one inlet and one outlet. Anything that passes through is then filtered into a small chamber inside of the catch can. The filter is placed 45° in the direction of the flow and in a manner that only fluid can pass through. The chamber with the filter is detachable and can be removed by unscrewing from the base. The catch can is then directing flow back to the fluid reservoir.



Figure 23: Particle capture can.

Each can is emptied and the particles are then rinsed to remove glycerin. Glycerin does not evaporate, if it is not completely removed in the rinsing process the particles will never dry completely. Glycerin is also troublesome to handle because of its sticky nature making particles hard to separate. At this point all particle sizes are mixed together. Most of them can easily be counted because of the small number of particles, but the descending aorta catch can is typically filled with 60-70% of the particles released. These are separated by being placed in a container that has 2.5 mm holes at the base and 4 mm holes at the lid which allows only 2 or 3.5 mm particles to fall. This provides a straightforward manner to counting particles and roughly shortened the counting and sorting process by 30 minutes over manual separation. A scale is used to find the mass of each set of particles. The mass of each

individual particle was determined by counting 50 particles, determining the mass of the collected particles, and then dividing by the number of particles counted. A small code was written in MathCAD that can be found in APPENDIX B: RELATIVE FLOW RATES where the masses were input for up to 5 runs and the number of particles is given for each run.

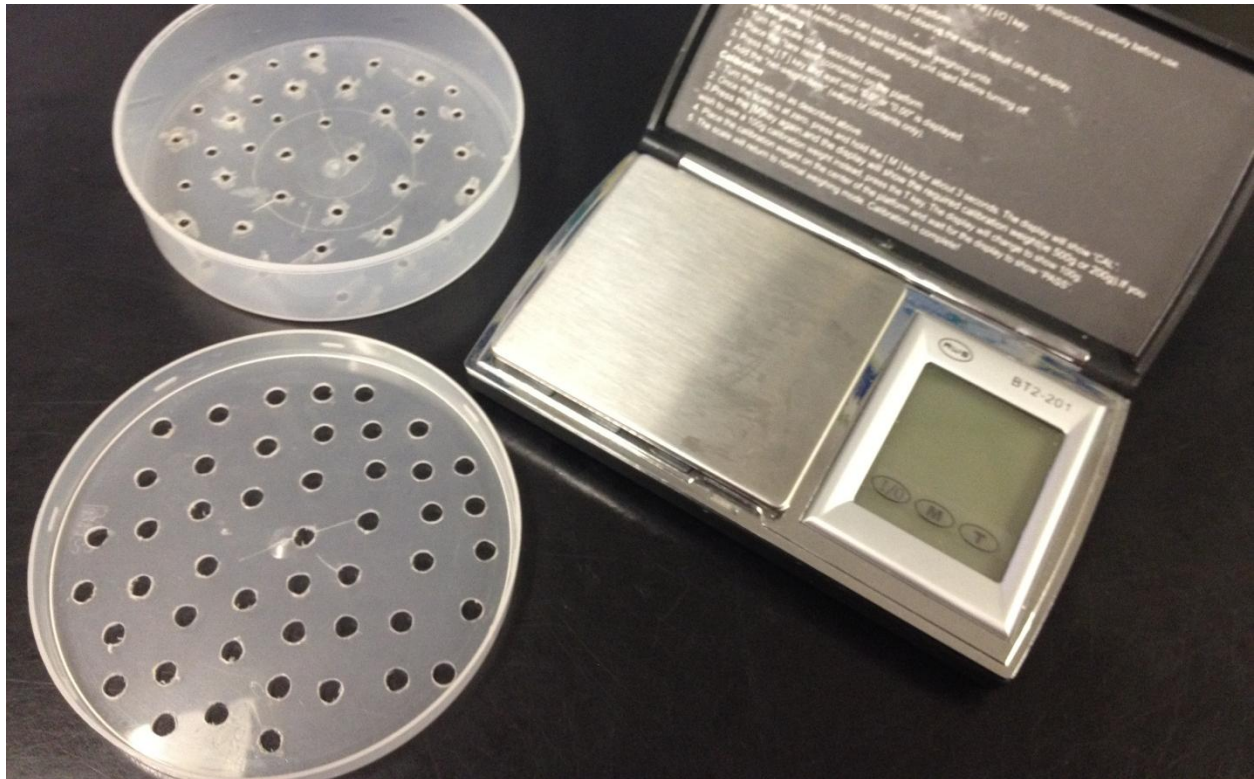


Figure 24: Particle separator and measurement device.

To visualize the particle streamlines, a high speed camera was used to capture the motion of the particles at 300 fps. When frames are being captured at such a high rate, a separate light source must be provided. The camera is mounted on a tripod and recordings were taken for each LVAD cannula configuration. These videos are edited and compared to the flow fields calculated by the CFD.

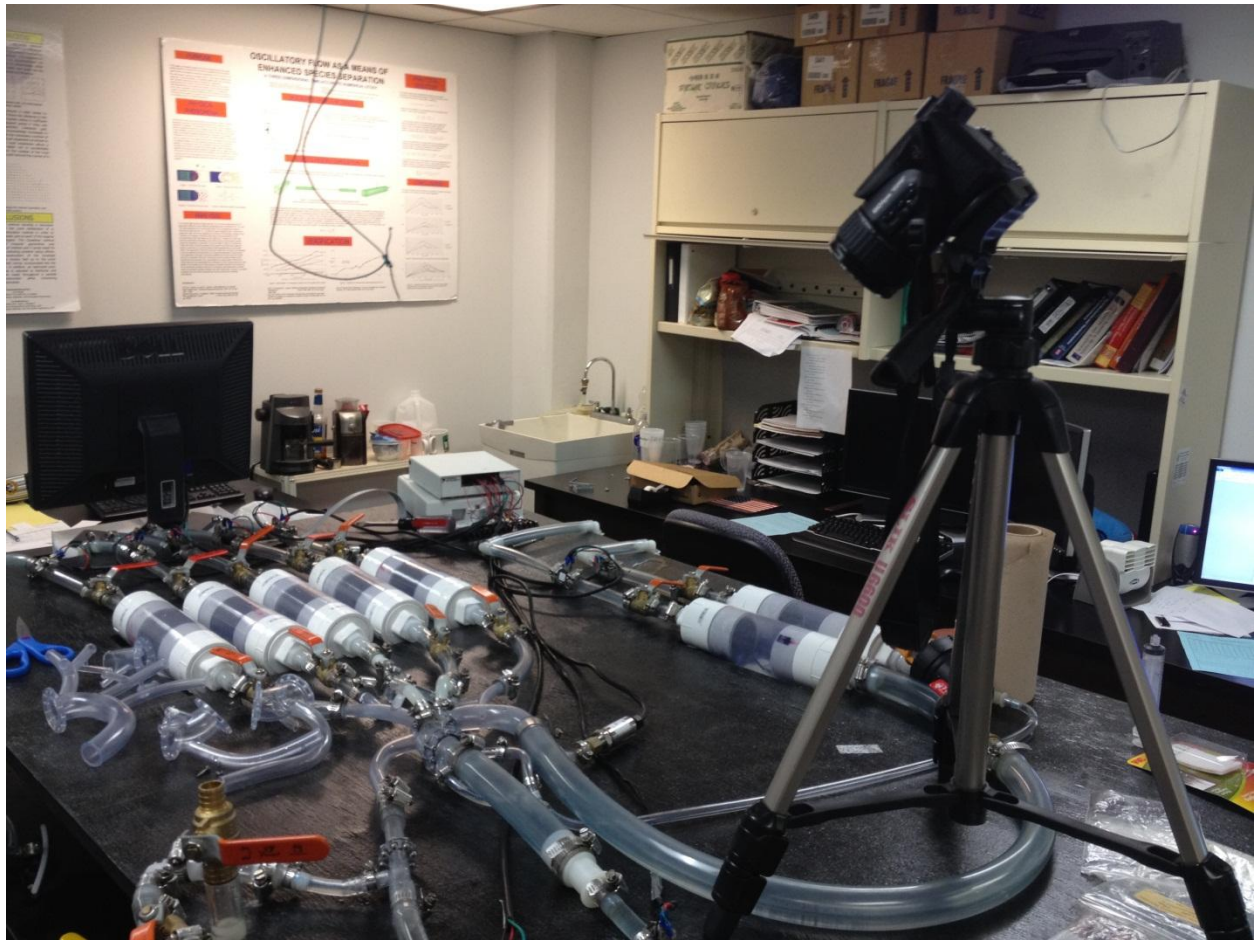


Figure 25: Camera apparatus for high FPS recordings of particles.

CHAPTER FOUR: RESULTS AND DISCUSSION

There are 9 possible LVAD cannula orientations that can be studied currently by the bench top experiment. Those configurations consist of the three standard configurations illustrated in Figure 26, those same configurations with a bypass connecting to the left carotid artery and the last three also from a bypass connecting to the innominate artery. In Figure 26, 0° represents the perpendicular configuration while 30° and 60° represent the intermediate and shallow configurations respectively. In addition to these 9 configurations, there are 3 different levels where the particles can be inserted into the system. These are labeled inside, centered and outside, see Figure 20. This is to simulate the variation where particles are released in the CFD, instead of just one fixed location. Particles were released and counted depending on which vessel to which they traveled. The particles going to LCA, RCA and VA's are considered to cause a thromboembolic event (stroke), thus the sum of the means were taken as an overall measure to determine the morbidity and mortality rates. This chapter includes the presentation and discussion of results.

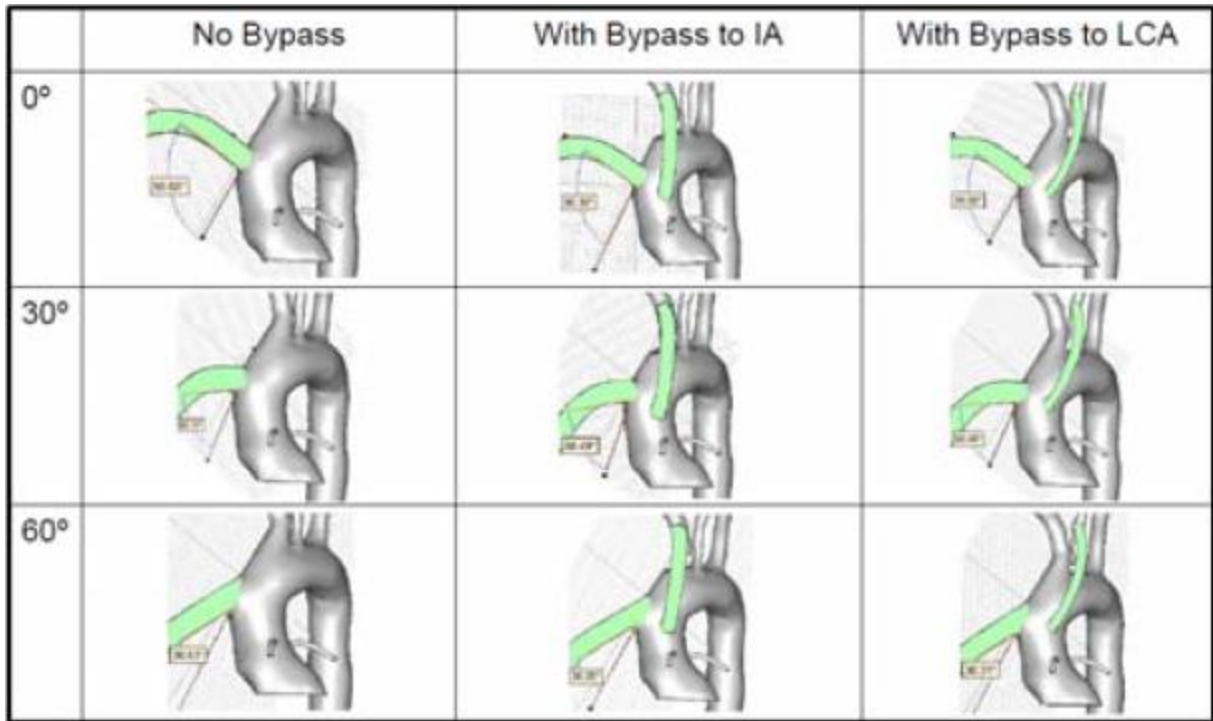


Figure 26: 9 different LVAD orientations.

Each LVAD cannula orientation features a flow field with different levels of recirculation zones due to the outflow VAD jet impingement onto the contralateral wall of the aortic arch. Based solely on geometry, particles cannot reach the innominate artery but because particles can be captured into the recirculation zone and then can subsequently be guided into the innominate artery. The recirculation zone is displayed by recording video of particles taken with a high speed camera at 300 frames per second. Screenshots of the recording are taken and compiled to show the time lapse of a particle traveling through the aortic arch and down surrounding vessels for each orientation.

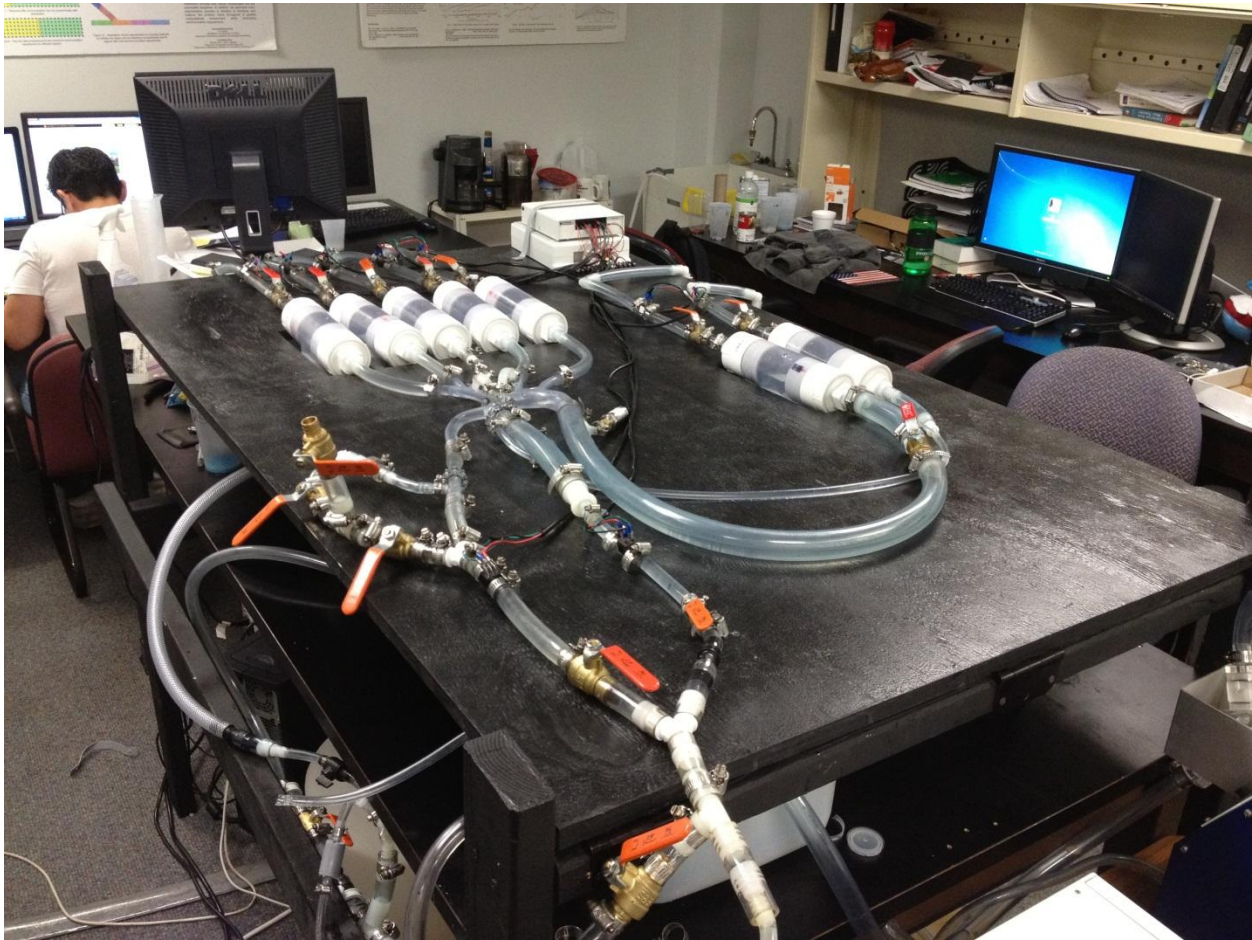


Figure 27: Bench top experiment apparatus.

4.1 Comparing Bench Top with CFD Results

The results were tabulated in excel, consisting of individual numbers of particles traveling to each terminal vessel. These are then converted into percentages by dividing the number of particles that traveled to that vessel by the total number of particles in a trial. The mean of five trials is calculated. The variance and standard deviation is calculated for each set of 5 runs and an error level is established for each means based on a 95% confidence level and assuming a normal distribution.

To gain insight into the particles behavior and resulting means, the Stokes number (St) was calculated. Stokes number is defined as the ratio of the particle response time, τ_p , to the convective time scale, τ_f , and indicates the relative importance of surface forces acting on a particle to the momentum of the particle. The Stokes number is calculated at a few points along the aortic arch using both CFD and bench top properties.

$$St = \frac{\tau_p}{\tau_f} = \frac{\rho_p d_p^2 U}{18\mu_f D} \quad (7)$$

The Stokes number is dependent on the diameter of particles, geometry, density of fluid and particles, and the velocity of the fluid. Since only viscosity and Reynolds number were matched, the density and velocity of the fluid is different than what was studied in CFD. This means that the Stokes number in the CFD and bench top are different. The Stokes number in the CFD is approximately 6% greater than the bench top. But since the difference in density was small, $\frac{\rho_{bench\ top}}{\rho_{CFD}} = 1.06$ and the geometry remained the same, the difference in magnitude of the Stokes numbers between the CFD and bench top is not significant, and the Stokes number computed from the CFD model can be used to identify behavior of particles in both the benchtop rig and the CFD model. The Stokes number governs the tendencies of particles that are suspended in fluid to follow streamlines or deviated from streamlines. If the Stokes number is less than 1, then particles are more likely to follow the streamlines because the surface forces entraining the particle dominate over the particle momentum. If the Stokes number is greater than 1, then particles are more likely to break free from the streamlines, especially at any bends or turns, because of the momentum of the particle dominates over the forces acting on the particle.

A CFD study using the flow properties of the bench top experiment was carried out to capture the flow field and to help understand the velocity magnitudes inside the aortic arch. The Stokes number described in the figure was calculated by either the average velocity at a section or by the range of the minimum and maximum velocity magnitude. The minimum and maximum was used to best describe the large disparity in velocity magnitudes caused by the jet exiting the cannula. This is done to provide a reference convective velocity for Stokes number calculations. The 2 mm and 5 mm particles are well described throughout the flow field by having a Stokes number much less than one and much greater than one respectively. The particle distributions for the 2 mm and 5 mm particles behave in a manner that is consistent on a case to case basis. However, the Stokes number of the 3.5 mm particles is near 1 through the aortic arch. This means that the particle tendencies neither follow the velocity streamlines nor break away from the velocity streamlines on a consistent basis. Resulting particle mean statistics determine that for the perpendicular and intermediate orientations that the 3.5 mm particles do behave similar to the 2 mm particles. For the shallow orientation, the 3.5 mm particles behave similar to the 5 mm particles. These observations have a strong correlation with the recirculation zone intensity of the perpendicular and intermediate cases.

Intermediate No Bypass Velocity Vectors Showing Stokes Number at Various Sections

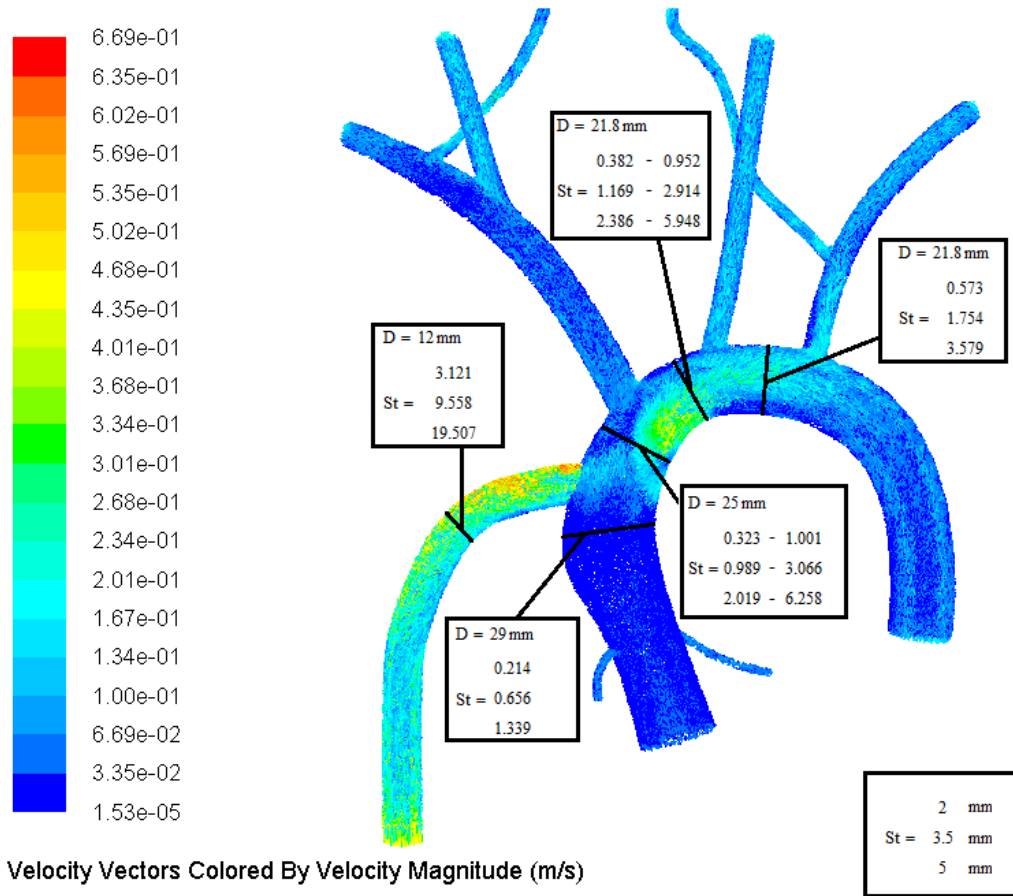


Figure 28: Stokes number at various locations in the aortic arch.

The configuration analyzed the most throughout the bench top study was the intermediate with no bypass. Runs were done from the centered, inside and outside particle injection locations. Originally the bench top was studied with 2, 4 and 5 mm particles. During a run, the 4 mm particles would get wedged inside the vertebral arteries, also 4 mm, and the run would have to be halted and the data set would be ruined. To tailor to this problem, the particles studied were changed from 4 mm to 3.5 mm which will not fit easily into the VA. The particle tracks for the CFD for each case were run again with the same flow field that the bench top study.

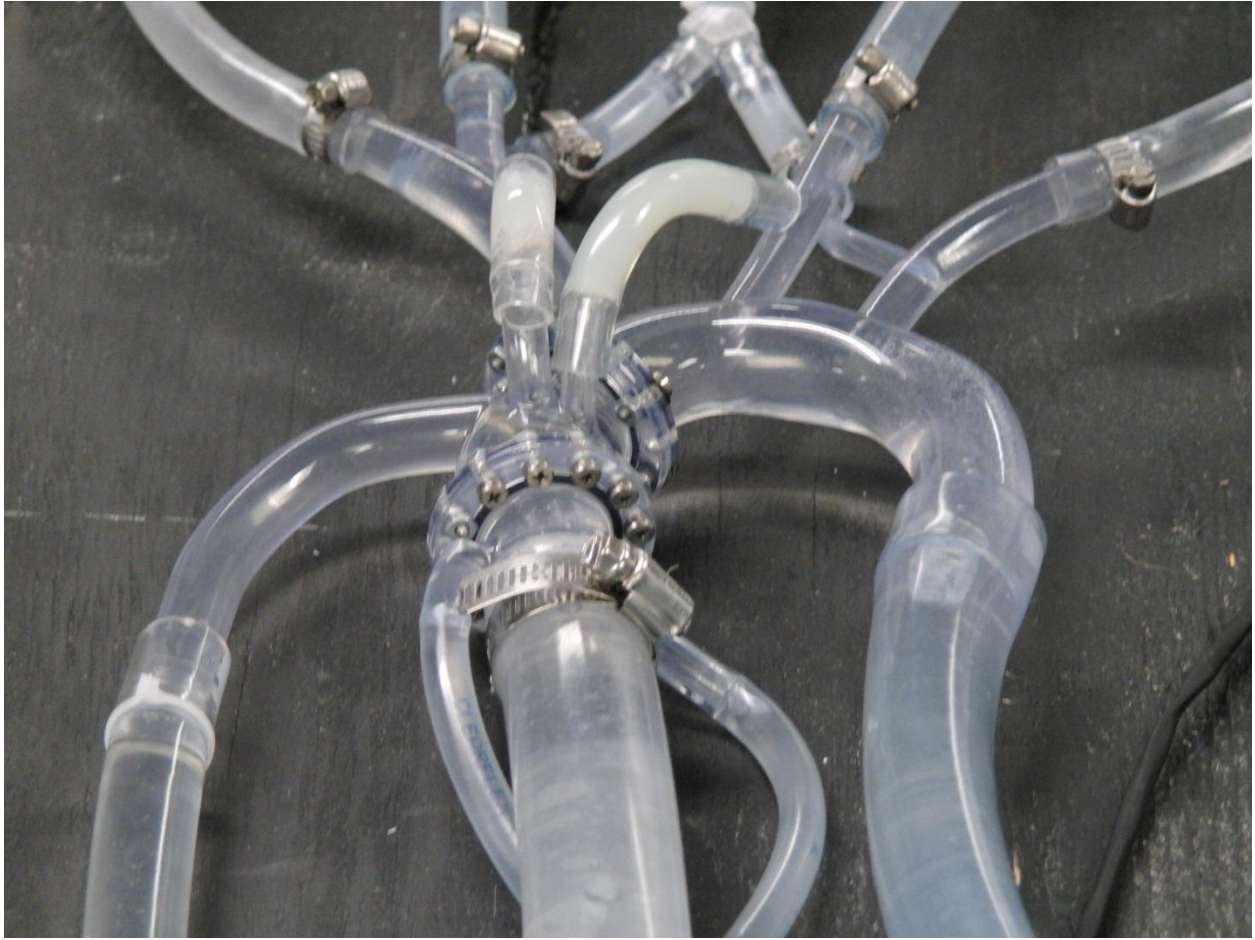


Figure 29: Intermediate LVAD cannula studied with no bypass.

Table 1: Intermediate No Bypass Centered Injection Configuration Results Compared to CFD.

Source	2 mm Thrombi (% reaching LCA, RCA and VA)	3.5 mm Thrombi (% reaching LCA, RCA and VA)	5 mm Thrombi (% reaching LCA, RCA and VA)	Overall (% reaching LCA, RCA and VA)
CFD	22.12±1.27	20.1±3.75	14.92±4.71	19.05±3.26
BT (centered)	21.71±2.49	20.96±1.19	15.15±2.98	19.26±2.35

Table 1 shows consistency of the means between the CFD embolism rates versus the bench top embolism rates. A comparison between means from the CFD and bench top is computed using the means from the 2, 3.5, 5 mm and overall. Statistical comparison of means is carried out using a 95% confidence limit and normal distribution, the null hypothesis, μ_0 , is that the means of embolism rates are equal and the alternative hypothesis is that the means are not equal.

Table 2: Testing criteria for null hypothesis, $\mu = \mu_0$.

Alternative hypothesis	Reject null hypothesis if:
$\mu \neq \mu_0$	$Z < -1.96$ or $Z > 1.96$

A comparison of means was done to justify the results between the centered injection configuration and the CFD for the intermediate LVAD cannula configuration with no bypass. This includes a comparison of the mean amount of particles that traveled to the LCA, RCA and VA for 2, 3.5 and 5 mm sized particles. A Z-score is calculated for a two-tailed test with a 95% confidence level. At a 95% confidence level the bounds for a normal distribution is $-1.96 \leq Z \leq 1.96$. A Z-score comparing the means from the CFD and the bench top are then calculated. A Z-score equal to 0 would show that the means are identical, therefore a Z-score that falls between $-1.96 \leq Z \leq 1.96$ results in a rejection of the alternative hypothesis. For the 2 mm particles, a comparison of means between the embolism rates 22.12 ± 1.27 and 21.71 ± 2.49 for CFD and bench top respectively, results in a Z-score equal to -0.345 and the alternative hypothesis is then rejected. A total of 6607 particles were released and tabulated in five trials for the CFD and 1496 particles were released, sorted and counted also in five trials for the bench top. The probability that a 2 mm particle will travel to the LCA, RCA or VA arteries is 22%. The probability is calculated by taking the

sum of the number of particles that traveled to the LCA, RCA and VA for both the CFD and bench top and dividing that by the sum of the total number of particles released. The Z-score for 2 mm particles lies within the bounds of the normal distribution, and it was located close to zero meaning that these means are very similar and there is no difference between the CFD and bench top. A sample calculation for comparing means can be seen in APPENDIX A: MEAN COMPARISON. For the 3.5 mm, a comparison of means between 20.1 ± 3.75 and 20.96 ± 1.19 resulted in a Z-score of 0.75. A total of 6612 particles were tabulated for the CFD and 1511 released for the bench top. The probability that a 3.5 mm particle will cause thromboembolism is 20.3%. Again, this is within the normal distribution and the alternative hypothesis is rejected. For the 5 mm particles, a comparison of means between 14.92 ± 4.71 and 15.15 ± 2.98 lead to a Z-score of 0.226 and the alternative hypothesis is rejected. A total of 6612 and 1510 particles were released for the CFD and bench top respectively with a probability of 15%. Lastly, the average of the means is taken and then the Z-score is calculated. A comparison of means is then taken between 19.05 ± 3.24 and 19.26 ± 2.35 and the calculated Z-score is 0.324. A total of 19831 particles were used to compile the results for the CFD and 4517 were used in the bench top. This is within the acceptable range of the normal distribution and the alternative hypothesis is rejected. All means tested for the centered injection configuration resulted in no agreements with the alternative hypothesis which states that the means are indeed equal and there is no difference between the results from the CFD and the intermediate with no bypass for the centered injection bench top configuration.

To ascertain if any difference exists due to various injection locations, the inside and outside were ran with the intermediate no bypass case. Particles released for these two injection configurations were 2, 3.5 and 5 mm.

Table 3: Intermediate No Bypass Summarized Results.

Source	2 mm Thrombi (% reaching LCA, RCA and VA)	3.5 mm Thrombi (% reaching LCA, RCA and VA)	5 mm Thrombi (% reaching LCA, RCA and VA)	Overall (% reaching LCA, RCA and VA)
CFD	22.12±1.27	20.10±3.75	14.92±4.71	19.05±3.26
BT (centered)	21.71±2.49	20.96±1.19	15.15±2.98	19.26±2.35
BT (inside)	21.98±6.88	21.31±2.49	15.75±3.44	19.66±4.67
BT (outside)	21.65±5.85	21.39±2.32	14.35±3.57	19.10±4.18
BT (average)	21.71±5.02	21.22±2.00	15.06±3.32	19.31±3.71

Similar to the centered configuration, a comparison of means was done between the inside injection configuration and the CFD for the intermediate LVAD cannula configuration with no bypass. For the 2 mm particles, a comparison of means between the embolism rates 22.12±1.27 and 21.98±6.88 for CFD and bench top respectively, results in a Z-score equal to -0.117 and the alternative hypothesis, that the means are not equal, is then rejected. A total of 6607 particles were released and tabulated in five trials for the CFD and 1479 particles were released for the bench top. The probability that a 2 mm particle will travel to the LCA, RCA or VA arteries is 22.1%. For the 3.5 mm, a comparison of means between 20.1±3.75 and 21.31±2.49 resulted in a Z-score of 1.039. A total of 6612 particles were tabulated for the CFD and 1458 released for the bench top. The probability that a 3.5 mm particle will cause thromboembolism is 20.3%. Again, this is within the normal distribution and the alternative hypothesis is rejected. For the 5 mm particles, a comparison of means between 14.92±4.71 and 15.75±3.44 lead to a Z-score of 0.810 and the alternative hypothesis is rejected. A total of 6612 and 1496 particles were released for the CFD and bench top respectively with a probability of 15.1%. Lastly, the average of the means is taken and then the Z-score is calculated. A comparison of means is then taken between 19.05±3.24 and 19.66±4.67 and the calculated Z-score is 0.933. A total of 19831 particles were used to compile the results for the CFD and 4437 were used in the bench top. This is within the

acceptable range of the normal distribution and the alternative hypothesis is rejected. All means tested for the inside injection configuration resulted in agreement with the null hypothesis which states that the means are indeed equal and there is no difference between the results from the CFD and the intermediate with no bypass for the inside injection bench top configuration.

Similarly to the previous two injection configurations, the outside injection configuration was compared to the mean embolism rates from the CFD for the intermediate no bypass LVAD cannula configuration. Starting with the 2 mm particles, a comparison of means between 22.12 ± 1.27 and 21.65 ± 5.85 for CFD and bench top respectively resulted in a Z-score of -0.579 and the alternative hypothesis, that the means are not equal, is rejected. The total number of particles associated to the five trials simulated by the CFD was 6607 and for the bench top a total of 1479 particles were released. Additionally, the overall probability for 2 mm particles reaching the LCA, RCA, and VA is 22%. For the 3.5 mm, a comparison of means is taken between 20.1 ± 3.75 and 21.39 ± 2.32 which resulted in a Z-score of 1.107. This Z-score is still within the normal distribution and the alternative hypothesis is then rejected. A total of 6612 particles were tabulated for the CFD and 1457 analyzed for the bench top. The probability that embolism will occur for 3.5 mm particles for both the CFD and bench top combined is 20.3%. For the 5 mm particles, a comparison of means between 14.92 ± 4.71 and 14.35 ± 3.57 lead to a Z-score of -0.579 and the alternative hypothesis is rejected. A total of 6612 and 1496 particles were released for the CFD and bench top respectively with a probability of 14.8%. A comparison of overall means is then taken between 19.05 ± 3.24 and 19.1 ± 4.18 and the calculated Z-score is -0.061. A total of 19831 particles were used to compile the results for the CFD and 4431 were used in the bench top and had a probability of 19%. Correspondingly with the 2, 3 and 5 mm particles the overall Z-score was well within the normal distribution and the alternative hypothesis is rejected. All means tested for the

outside injection configuration resulted in agreement with the null hypothesis which states that the means are indeed equal and there is no difference between the results from the CFD and the intermediate with no bypass for the inside injection bench top configuration.

Since the centered, inside and outside injection configuration both concluded that the alternative hypothesis should be rejected, a mean comparison was done for all particle sizes between the centered and inside, centered and outside and inside and outside configurations themselves. This was completed to see whether or not there is a difference in the results produced by the separate injection configurations.

A comparison of means between the centered and inside injection configurations were completed next. For the 2 mm particles, the means being compared were 21.71 ± 2.49 and 21.98 ± 6.88 for the centered and inside injection configurations respectively. This resulted in a Z-score equal to -0.178 and a rejection of the alternative hypothesis. The probability for the combined injection configurations was 21.8%. For the 3.5 mm particles, the means being compared were 20.96 ± 1.19 and 21.31 ± 2.49 . This comparison resulted in a Z-score being equal to -0.235 and the alternative hypothesis being rejected. The probability for the combined injection configurations was calculated to be 21.1%. For the 5 mm particles, the means being compared were 15.15 ± 2.98 and 15.75 ± 3.44 . This comparison resulted in a Z-score being equal to -0.445 and the alternative hypothesis being rejected. The probability for the combined injection configurations was calculated to be 15.4%. Lastly, the overall means were compared 19.26 ± 2.35 and 19.66 ± 4.67 . The Z-score calculated for the overall mean was -0.478 and the alternative hypothesis were then rejected. For all four mean comparisons, the alternative hypothesis was rejected. This states that there is no difference in where the particles are released from.

A comparison of means between the centered and outside injection configurations were completed next. For the 2 mm particles, the means being compared were 21.71 ± 2.49 and 21.65 ± 5.85 for the centered and outside injection configurations respectively. This resulted in a Z-score equal to -0.186 and a rejection of the alternative hypothesis. The probability for the combined injection configurations was 21.6%. For the 3.5 mm particles, the means being compared were 20.96 ± 1.19 and 21.39 ± 2.32 . This comparison resulted in a Z-score being equal to -0.287 and the alternative hypothesis being rejected. The probability for the combined injection configurations was calculated to be 21.2%. For the 5 mm particles, the means being compared were 15.15 ± 2.98 and 14.35 ± 3.57 . This comparison resulted in a Z-score being equal to 0.618 and the alternative hypothesis being rejected. The probability for the combined injection configurations was calculated to be 14.8%. Lastly, the overall means were compared 19.26 ± 2.35 and 19.10 ± 4.18 . The Z-score calculated for the overall mean was 0.192 and the alternative hypothesis was then rejected. For all four mean comparisons, the alternative hypothesis was rejected. This states that there is no difference in where the particles are released from.

The comparison between the inside and outside injection configurations were completed first. For the 2 mm particles, the means being compared were 21.98 ± 6.88 and 21.65 ± 5.85 for the inside and outside injection configurations respectively. This resulted in a Z-score equal to 0.363 and a rejection of the alternative hypothesis. The probability for the combined injection configurations was 21.7%. For the 3.5 mm particles, the means being compared were 21.31 ± 2.49 and 21.39 ± 2.32 . This comparison resulted in a Z-score being equal to -0.053 and the alternative hypothesis being rejected. The probability for the combined injection configurations was calculated to be 21.3%. For the 5 mm particles, the means being compared were 15.75 ± 3.44 and 14.35 ± 3.57 . This comparison resulted in a Z-score being equal to 1.118 and the alternative hypothesis being rejected. Lastly, the overall means were compared

19.66±4.67 and 19.1±4.18. The Z-score calculated for the overall means was 0.775 and the alternative hypothesis was rejected. For all four mean comparisons, the alternative hypothesis was rejected. This states that there is no difference in where the particles are released from. For the remaining results, only the centered injection configuration will be studied.

Table 4: Summary of centered, inside and outside injection configurations Z Scores.

Source	2 mm Thrombi (Z Score)	3.5 mm Thrombi (Z Score)	5 mm Thrombi (Z Score)	Overall (Z Score)
Centered vs. Inside	0.178	-0.235	-0.445	-0.478
Centered vs. Outside	0.186	-0.287	0.618	0.192
Inside vs. Outside	0.363	-0.053	1.118	0.775

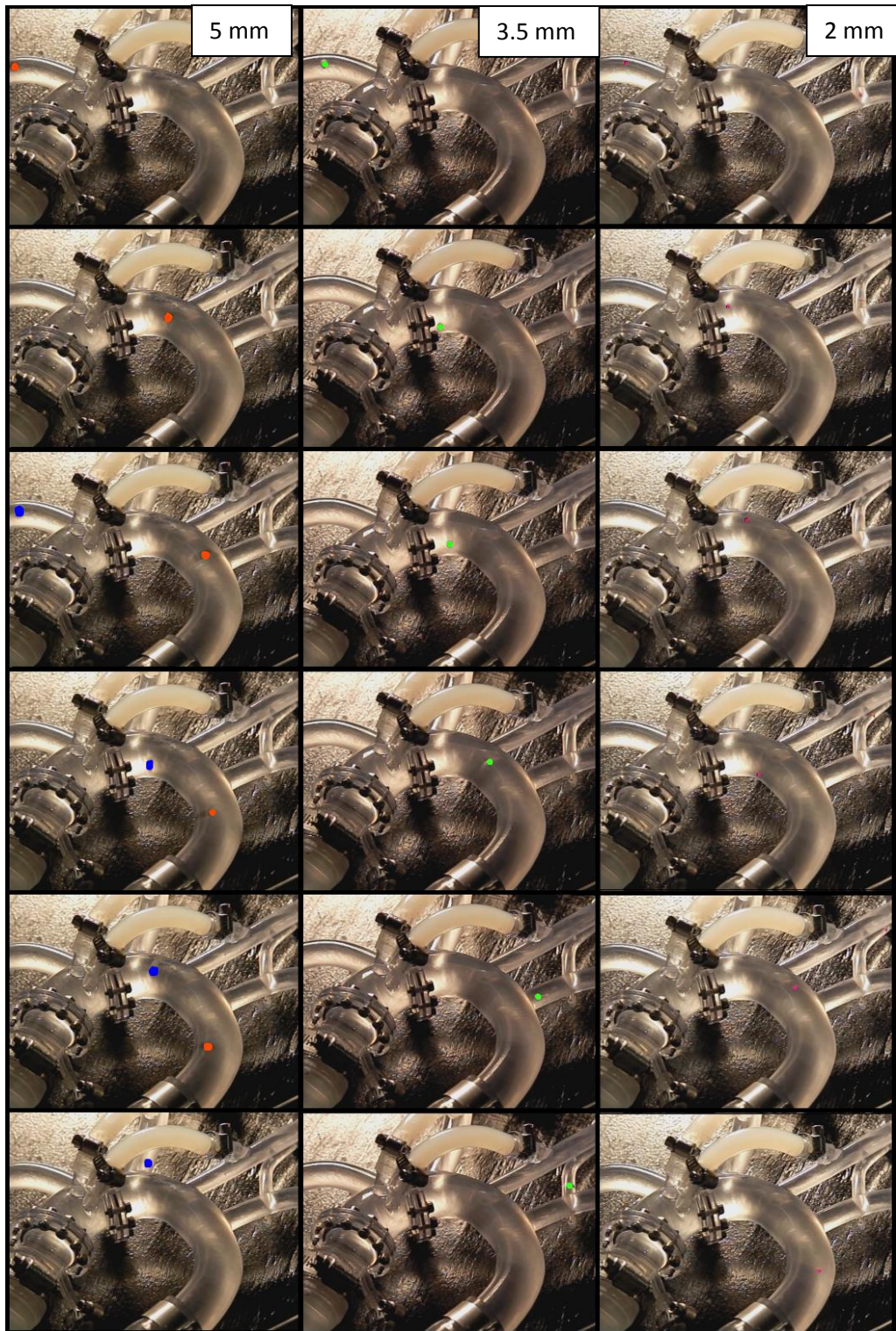


Figure 30: Particle traces for intermediate with no bypass.

The figure above is to describe the particle path after it has entered the flow field for the intermediate with no bypass orientation. Video was taken from a high speed camera at 300 frames per second. To illustrate the video taken, screen captures are displayed of a particle path from start to finish. To better detail the particle path in the flow field, the particle was highlighted manually. The particle path was chosen at in a manner to capture something out of the ordinary in the flow field rather than show something with no interaction. For example, the blue 5 mm particle in the first column of pictures travels into the aortic arch, well passed the innominate artery and is quickly captured by the recirculation zone in the ascending aorta. This particle then proceeds to travel against the direction of the flow and into the innominate artery. Similarly for the 2 mm particle in the third column, the particle being observed is directed towards the top of the aortic arch and then its position oscillates from the bottom, back to the top and eventually travelling down the descending aorta. The particle paths displayed by the video captured of the data set are in agreement with the flow field solved by the CFD.

Table 5: Perpendicular with No Bypass Compared to CFD.

Source	2 mm Thrombi (% reaching LCA, RCA and VA)	3.5 mm Thrombi (% reaching LCA, RCA and VA)	5 mm Thrombi (% reaching LCA, RCA and VA)	Overall (% reaching LCA, RCA and VA)
CFD	18.14±3.69	17.89±4.06	25.05±3.18	20.36±3.64
Bench Top	19.58±3.7	18.88±5.71	20.52±2.01	19.66±4.10

The next LVAD cannula orientation under consideration was the perpendicular with no bypass. The process of determining whether or not this orientation is in agreement with the CFD outcome was similar to the study of the intermediate orientation. The only difference between the two is that only one injection configuration was studied for the perpendicular with no bypass case. The perpendicular flow field shows the strongest recirculation zone of the three different LVAD cannula configurations. This is because the jet from the cannula impinges directly on the left lateral ascending aorta wall.

Particles often captured in the recirculation zone and can be sent to undesirable locations. For the 2 mm particles, the mean of particles reaching the LCA, RCA and VA are 18.14 ± 3.69 and 19.58 ± 3.7 for the CFD and bench top respectively. A comparison of means statistic is done and the resulting Z-score is 1.298 which is still within the normal distribution and the alternative hypothesis can be rejected. The probability that 2 mm particle will reach the LCA, RCA and VA combined for the CFD and bench top is 18.4%. The total number of 2 mm particles used this study was 6730 for CFD and 1490 for the bench top. For the 3.5 mm particles, the means being compared are 17.89 ± 4.06 and 18.88 ± 5.71 . This comparison resulted in a Z-score equal to 0.898 and the alternative hypothesis was rejected. The total probability that a 3.5 mm particle will result in embolism is 18.1%. For the 5 mm particles, the means being compared are 25.05 ± 3.18 and 20.52 ± 2.01 . The Z-score calculated was -3.715 and resulted in the alternative hypothesis being accepted. This is the first of any means compared that were not an accurate match between the CFD and bench top. The reasons for the deviations are from the CFD's ability to capture particles that travel down a vessel that has a smaller diameter than the particle. For the bench top, the 5 mm particle will have to occlude the inlet to the VA to be counted. When this occurs, particles are stopped from being released and the occlusion is removed and counted in real time. For the CFD, the particle is represented by an infinitely small point and does not take into account whether or not the diameter of the vessel is smaller than the diameter of the particle it is representing. Another difference between the CFD and bench top results is that the DA for 5 mm particles is 15.3% higher for the bench top. The probability for the CFD and bench top was 24.2%. The total number of 5 mm particles used for the CFD was 6371 and 1529 for the bench top. For the overall comparison, the means being compared are 20.36 ± 3.64 and 19.66 ± 4.1 . This resulted in a Z-score of -1.054 and the rejection of the alternative hypothesis. The reason the alternative hypothesis was not rejected, even though 5 mm particles did not compare, because the means for the bench top 2 and 3.5 mm particles

were higher than the CFD and the 5 mm was lower which balanced the overall means. The probability that a particle will reach the LCA, RCA and VA for the perpendicular with no bypass was 20.2%. The total number of particles released for this study was 19079 for the CFD and 4527 for the bench top.

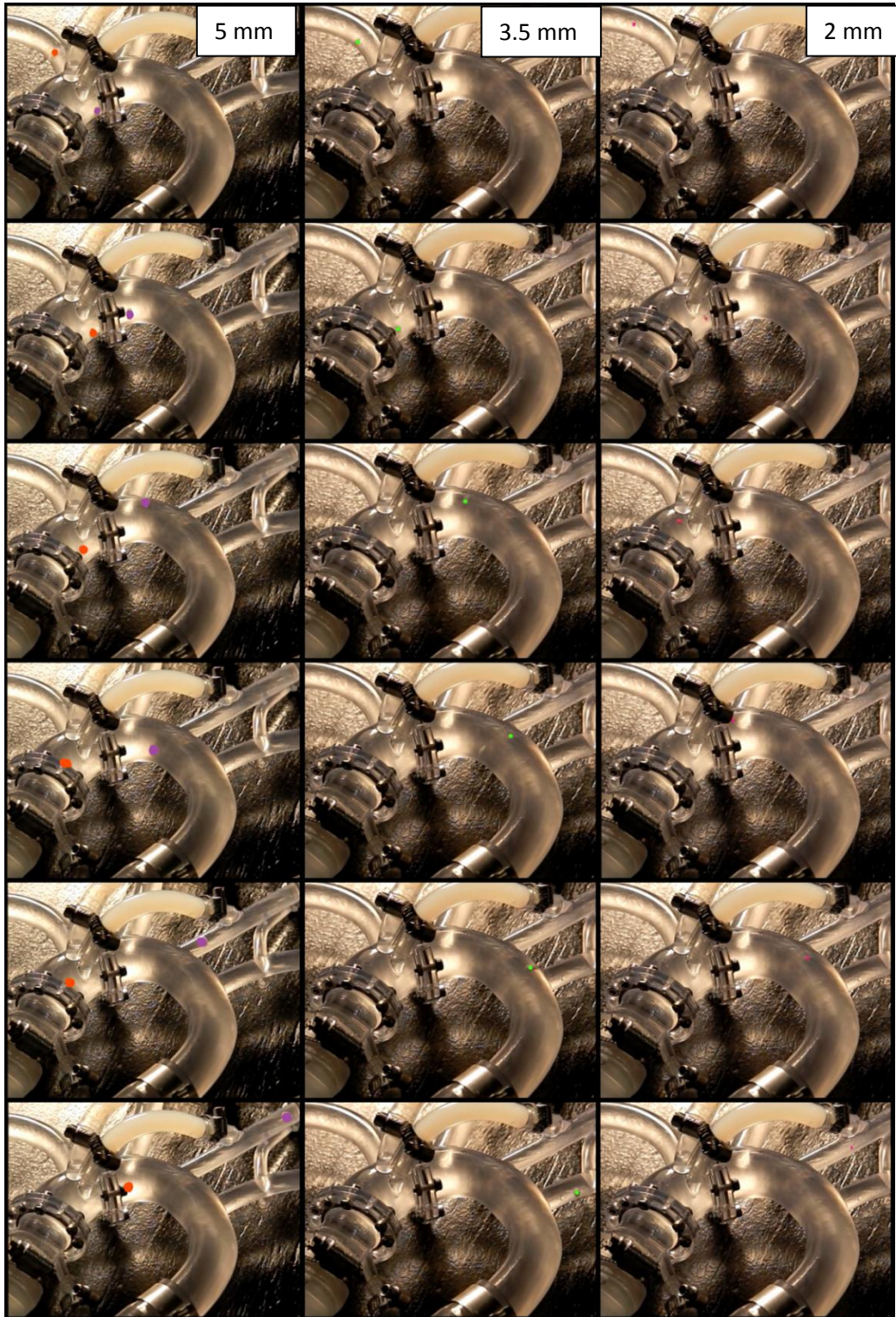


Figure 31: Particle tracks for perpendicular no bypass.

Table 6: Shallow with No Bypass Compared to CFD.

Source	2 mm Thrombi (% reaching LCA, RCA and VA)	3.5 mm Thrombi (% reaching LCA, RCA and VA)	5 mm Thrombi (% reaching LCA, RCA and VA)	Overall (% reaching LCA, RCA and VA)
CFD	12.91±1.95	8.64±3.32	9.63±3.18	10.39±2.13
Bench Top	14.68±2.18	8.72±4.02	7.01±3.17	10.14±3.21

The LVAD cannula orientation being studied is the shallow with no bypass. This orientation directs the jet from the cannula down the aortic arch with a much reduced impingement on the left lateral wall of the aorta. There is a much smaller recirculation zone than the previous orientations studied based on the direction of the jet. From these observations, this orientation should show the fewest amount of particles traveling down the innominate artery. For the 2 mm particles, the mean of particles reaching the LCA, RCA and VA are 12.91±1.95 and 14.68±2.18 for the CFD and bench top respectively. A comparison of means statistic is done and the resulting Z-score is 1.909 which is still barely within the normal distribution and the alternative hypothesis can be rejected. The probability that 2 mm particle will reach the LCA, RCA and VA combined for the CFD and bench top is 13.1%. The total number of 2 mm particles used this study was 10101 for CFD and 1529 for the bench top. For the 3.5 mm particles, the means being compared were 8.64±3.32 and 8.72±4.02. This comparison resulted in a Z-score being equal to 0.104 and the alternative hypothesis being rejected. The probability for the 3.5 mm particles was calculated to be 8.7%. The total number of 3.5 mm particles used this study was 10107 for CFD and 1546 for the bench top. For the 5 mm particles, the means being compared are 9.63±3.18 and 7.01±3.17. The Z-score calculated was -3.267 and resulted in the alternative hypothesis being accepted. For both shallow and perpendicular with no bypass the 5 mm particles did not behave as in a manner that is comparable to the CFD. The reasons for the deviations lay heavily on the

distribution of particles that traveled to the vertebral arteries. As described for the perpendicular with no bypass case, the particles in the CFD can travel down a vessel that is smaller diameter whereas with the bench top it must be occluded. A majority of the occlusions happen when the particle travels through the innominate artery and rarely when the particle travels to the LSA. The probability for 5 mm particles for the CFD and bench top was 9.3%. The total number of particles released for the CFD was 10108 and 1505 for the bench top. For the overall comparison, the means being compared are 10.39 ± 2.13 and 10.14 ± 3.21 . This resulted in a Z-score of -0.518 and the rejection of the alternative hypothesis. The reason the alternative hypothesis was still rejected, even though 5 mm particles were not comparable, was because the mean for the bench top 2 mm particles were higher than the CFD and the 5 mm was lower which balanced the overall means. The probability that a particle will reach the LCA, RCA and VA for the perpendicular with no bypass was 10.4%. The total number of particles released for this study was 30316 for the CFD and 4580 for the bench top.

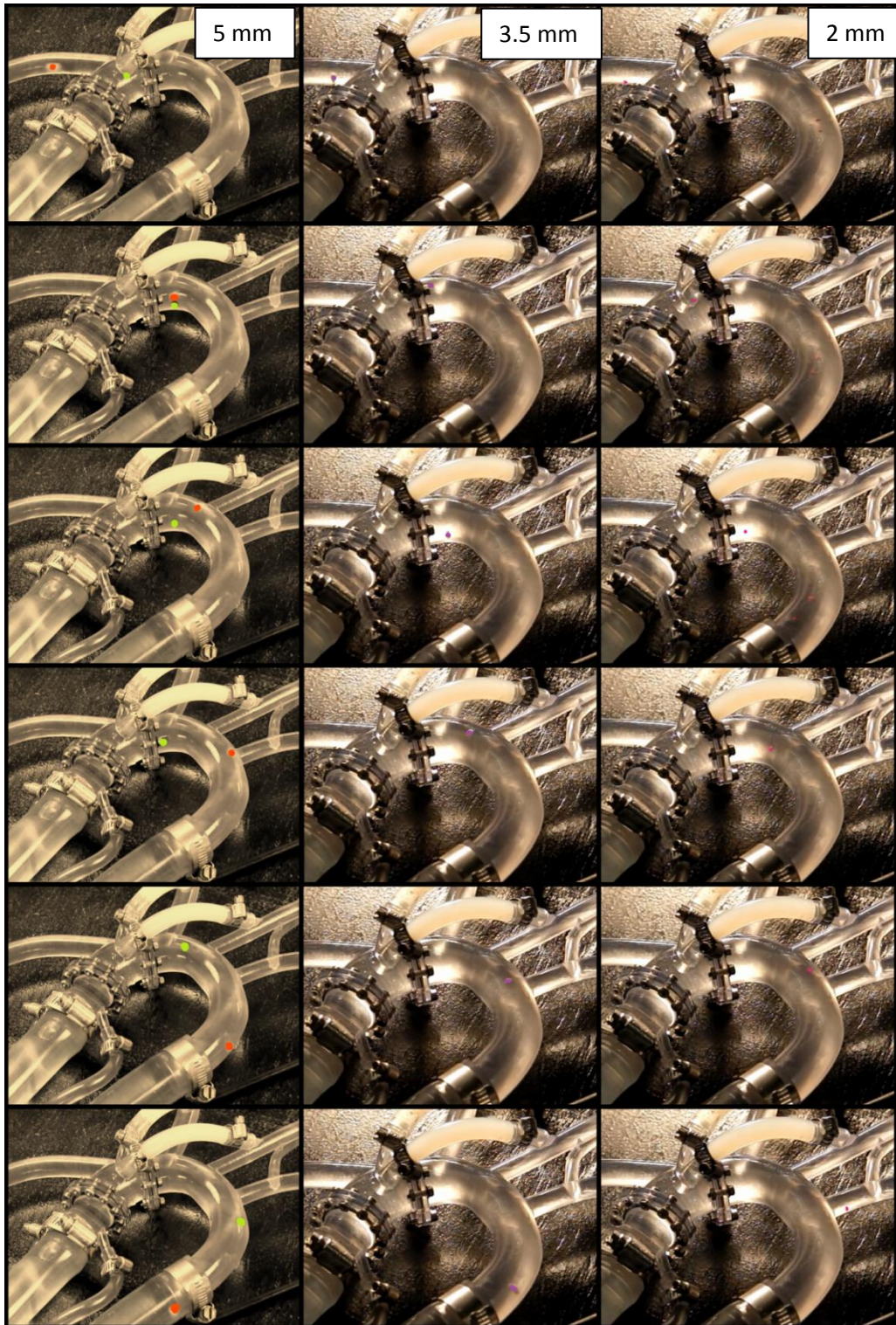


Figure 32: Particle tracks for shallow no bypass.

4.2 Bench Top Results

Table 7: Summarized Results for LCA bypass.

Orientation	2 mm Thrombi (% reaching LCA, RCA and VA)	3.5 mm Thrombi (% reaching LCA, RCA and VA)	5 mm Thrombi (% reaching LCA, RCA and VA)	Overall (% reaching LCA, RCA and VA)
Perpendicular	17.5±3.05	15.16±2.05	12.95±2.68	15.22±2.62
Intermediate	15.74±4.4	15.42±3.91	9.47±2.25	13.55±3.64
Shallow	13.42±5.38	8.52±2.18	4.71±2.13	10.14±3.21

The LCA was occluded by injecting silicone into the vessel which will only allow flow through the bypass that is located beneath the LVAD cannula jet. This placement gives particles the best chance to not travel down the bypass graft. Similar to the innominate artery, the only way particles can travel down the LCA bypass is if they are entrained into the recirculation zone caused by the jet impinging on the left lateral wall of the ascending aortic arch. When designing the rapid prototype model, the LCA bypass had to be moved slightly to accommodate the innominate artery bypass configuration as well as the flanged connections used for changing each of the orientations.

Having established that the bench top results do indeed provide results that are in agreement with the CFD models for the cases with no bypass, it was however, observed that the placement of the LCA bypass produces significantly different results between bench top and CFD. A CFD study with the three orientations and LCA bypass was conducted and it was shown that there was little improvement when the bypass was added. However, the bench top did show improvements. Other than the geometry, there is no factor that would cause the particle distribution to not be in conjunction with the computational model. As expected, the LVAD cannula orientation with the largest amount of recirculation proved to have the highest embolization rates and the lowest recirculation showed the lowest rates.



Figure 33: Shallow with LCA bypass and occluded LCA.

Comparing to the perpendicular configuration with no bypass to the configuration with a LCA bypass, it is noticed that all sizes had a significant reduction in the probability that particles will travel to the LCA, RCA and VA. For the 2 mm particles, there was a 10.6% reduction in embolization rates after the bypass was added. Additionally, it was observed that there was a 25.7% (3.64) increase in particles that traveled to the RCA and VA but there was a significant reduction of 63.1% (5.71) in particles that traveled to the LCA. The increase in embolization rates to the RCA and VA was caused by the change in the flow field due to the location of the LCA bypass. The impinged jet from the cannula was slightly above the LCA bypass. The recirculation zone intensified because of the addition of the LCA bypass. The bypass caused fluid to exit from the aortic arch earlier than it did when there was no bypass. When

there was no bypass fluid was distributed much further down the flow field after the recirculation zone and the innominate artery. For the 3.5 mm particles, a 19.7% reduction occurred. Similar to the 2 mm particles, there was an increase in particles that traveled to the RCA and VA and a significant reduction to the LCA. The increase to the RCA and VA was 24.4% (3.23) and the reduction to the LCA was 78.3% (6.96). For the 5 mm particles, a 37% reduction was identified. A reduction of 29.6% (1.88) particles traveled to the LCA. It was noticed from the distribution of statistics that 5 mm particles had a higher tendency to travel down the DA and LSA when compared to the no bypass study. The overall mean reduction was 22.6%.



Figure 34: Particle tracks for perpendicular with LCA bypass.

Comparing the intermediate with LCA bypass to the average of the three studies done at different injection configurations for the intermediate with no bypass, it was also noticed that all sizes had a reduction in the probability that particles will travel to the LCA, RCA and VA. For the 2 mm particles, there was a 27.5% reduction in embolization rates when the bypass to the LCA was added. The particle distributions did slightly change, except for the LCA which noticed an 83.6% (8.02) reduction in 2 mm particles that traveled to that outlet. For the 3.5 mm particles, a similar reduction of 27.3% in the reduction of particles that traveled to the LCA, RCA and VA. A reduction of 93.7% (10.3) was noticed of 3.5 mm particles that traveled to the LCA. For the intermediate with no bypass, there was a 2.2% reduction in particles traveling to LCA, RCA and VA between 2 and 3.5 mm particles compared to a 2.0% reduction for 2 and 3.5 mm particles when the LCA bypass was added. Also for 2 and 3.5 mm particles, there was an increase in the number of particles that traveled to the RCA and VA. This follows the same trend as the perpendicular case. For the 5 mm particles, there was a 37.1% reduction. A reduction of 91.5% (7.23) was noticed of 5 mm particles that traveled to the LCA. It is also noticed that a majority the 5 mm particles that normally would have traveled down the LCA, when there was no bypass, made their way do the DA since the LCA is now occluded for the study with the bypass. For the overall, there was a 19.5% reduction. Since the intermediate orientation has a lesser recirculation zone than the perpendicular, because of the impingement of the jet, fewer particles had been entrained by it. This observation is enforced by the difference in the number of particles that traveled down the LCA bypass when compared to the perpendicular configuration which has the stronger recirculation zone.

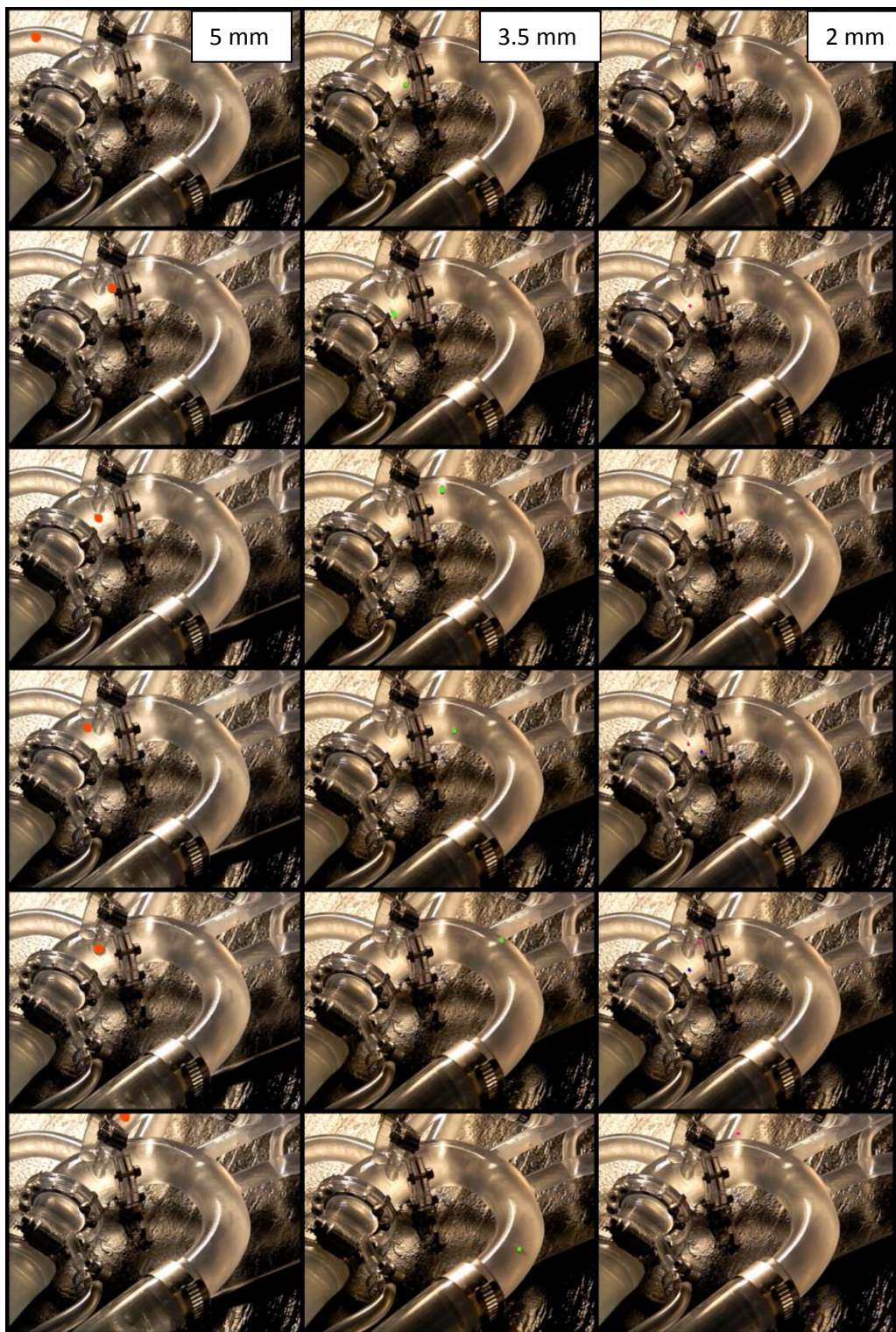


Figure 35: Particle traces for intermediate with LCA bypass.

Comparing the shallow orientation with LCA bypass to the shallow with no bypass, it was also noticed that all sizes had a reduction in the probability that particles will travel to the LCA, RCA and VA. These reductions were not as significant as the other two orientations, but the shallow configuration shows lower overall embolism rates. For the 2 mm particles, the reduction was 8.6% (1.26). In all 5 trials, only 4 2 mm particles traveled down the LCA bypass which leads to a 95.1% reduction (5.05). For the 3.5 mm particles, there was no reduction in particles that traveled to the RCA, LCA and VA. No 3.5 mm particles traveled down the LCA bypass. For the 2 and 3.5 mm particles, there was also an increase in the particles that traveled to the RCA and VA which is similar to both previous LCA bypass cases studied. The distributions of particles to the outlets are very similar when the RCA, LCA and VA are excluded. For the 5 mm particles, there was a 32.8% reduction. Also, no particles traveled through the LCA bypass. For the overall, an 11.8% reduction occurred.



Figure 36: Particle tracks for shallow with LCA bypass.

All bench top results show the same trend in particle distributions when compared to the CFD. For every case except perpendicular with no bypass, the 2 mm particles have the highest embolism rates. This is followed by a decrease in embolism rates for 3.5 mm particles. Similarly, the 5 mm particle embolism rates decreased even further. The 5 mm particles show the lowest embolism rates. This is in concurrence with the Stokes number calculations. The smaller the particle, the likelihood that a particle will follow the streamlines is high. If a particle is following the flow stream lines, it could easily reach the LCA, RCA or VA. For the largest particles, the tendency to break away from the streamlines typically will send them down the LSA or DA. For our purpose the LSA and DA are considered the least deleterious end vessel endpoints for thrombi.

Of all the cases studied, the shallow orientation with LCA bypass had the lowest overall embolism rate at 10.14 ± 3.21 . The shallow with LCA bypass also had the lowest embolism rates for the 2, 3.5 and 5 mm particles. The embolism rate of 4.71 ± 2.13 for the 5 mm particles was the lowest of any particle size for any configuration. The shallow orientation shows the best results because of the direction of the jet from the cannula into the aortic arch. Based on the geometry, any particle entering the flow field is propelled past the innominate artery unless caught into the recirculation zone. The shallow orientation has the smallest recirculation zone and thus the lowest embolism rates. When the bypass is added, any particle that was fired past the innominate artery would no longer have a chance to enter the LCA. This is why there is a reduction in embolism rates when the bypass is added.

Table 8: Summary of Results.

Orientation Bypass Injection	2 mm	3.5 mm	5 mm	Overall
Intermediate No Bypass Centered	21.71±2.49	20.96±1.19	15.15±2.98	19.26±2.35
Z-Score	-0.35	0.75	0.23	0.32
Intermediate No Bypass Inside	21.98±6.88	21.31±2.49	15.75±3.44	19.66±4.67
Z-Score	-0.117	1.039	0.810	0.933
Intermediate No Bypass Outside	21.43±5.7	21.39±2.32	14.29±3.55	19.01±4.1
Z-Score	-0.579	1.107	-0.620	-0.061
Intermediate No Bypass Averaged	21.71±5.02	21.22±2.00	15.06±3.32	19.31±3.71
Z-Score	-0.512	1.437	0.203	0.479
Perpendicular No Bypass Centered	19.45±3.52	18.88±5.71	20.52±2.01	19.62±4.04
Z-Score	1.298	0.898	-3.715	-1.054
Shallow No Bypass Centered	14.71±2.23	8.72±4.02	7.01±3.17	10.15±3.22
Z-Score	1.909	0.104	-3.267	-0.518
Intermediate LCA Bypass Centered	15.74±4.4	15.42±3.91	9.47±2.25	13.55±3.64
Perpendicular LCA Bypass Centered	17.5±3.05	15.16±2.05	12.95±2.68	15.22±2.62
Shallow LCA Bypass Centered	13.42±5.38	8.52±2.18	4.71±2.13	8.94±3.57

CHAPTER FIVE: CONCLUSION

The bench top experiment provides an accurate representation of the CFD models. Either the bench top experiment or the computational model can be used to determine whether or not the LVAD cannula orientation or bypass connection can be deemed appropriate for surgical use. The percentage of particles traveling to lethal arteries in this experiment was significantly reduced when compared to the standard. The least promising configuration was the intermediate and perpendicular with no bypass which both approximately sent 19.64 ± 4.36 percent of particles to the LCA, RCA and VA. This was because of the large recirculation zones caused by the impingement of the jet from the LVAD cannula to the left lateral wall of the aortic arch. The best case of the experiment came from the shallow configurations, by a substantial amount at 10.15 ± 3.22 and 8.94 ± 3.57 for the shallow with no bypass and shallow with bypass respectively. The least amount of recirculation because of the small amount of impingement on the left lateral wall was the primary reason for the low percentages.

5.1 Observations

Particles can only travel down the IA when they are captured by the recirculation zone. Recirculation zones for all cases were intensified when the bypass connections were added. Since the recirculation zone for the shallow with bypass orientation was so weak and the position of the bypass connection, almost no particles traveled to the LCA.

5.2 Future Work

The next logical step in this study is to utilize two pulsatile pumps to investigate the effects of pulsatile flow in the bench top experiment. This will establish if there is a significant difference in the number of particles traveling to the LCA, RCA, VA and coronaries between the steady mean flow model

and the more complex pulsatile model. Each pulsatile pump will mimic the aortic output for the ascending aorta or the waveform output from the LVAD pump.

APPENDIX A: MEAN COMPARISON

Ch. 9: Inferences Based on two Samples
 9.4: Inferences Concerning a Difference Between Population Proportions
 A Large-Sample Test Procedure

$$\text{Verify}(z) := \begin{cases} a \leftarrow \text{"accept alternative"} & \text{if } z \geq 1.96 \vee z \leq -1.96 \\ a \leftarrow \text{"reject alternative"} & \text{otherwise} \\ a \end{cases} \quad \text{Two Tailed 95\% Confidence Level}$$

New Case:

Intermediate No Bypass 2 mm – CENTERED

BT:	CFD:	
$n_1 := 1496$	$n_2 := 6607$	released
$p_1 := .2171$	$p_2 := .2212$	mean
$c_1 := n_1 \cdot p_1 = 324.782$	$c_2 := n_2 \cdot p_2 = 1461.468$	# of particles
$p := \frac{c_1 + c_2}{n_1 + n_2} = 0.22$	$q := 1 - p = 0.78$	Probability

$$z_{2\text{mm}} := \frac{p_1 - p_2}{\sqrt{p \cdot q \cdot \left(\frac{1}{n_1} + \frac{1}{n_2} \right)}} = -0.345$$

Verify($z_{2\text{mm}}$) = "reject alternative"

Intermediate No Bypass 3.5 mm – CENTERED

$n_1 := 1511$	$n_2 := 6612$	released
$p_1 := .2096$	$p_2 := .2010$	mean
$c_1 := n_1 \cdot p_1 = 316.706$	$c_2 := n_2 \cdot p_2 = 1329.012$	# of particles
$p := \frac{c_1 + c_2}{n_1 + n_2} = 0.203$	$q := 1 - p = 0.797$	Probability

$$z_{3.5\text{mm}} := \frac{p_1 - p_2}{\sqrt{p \cdot q \cdot \left(\frac{1}{n_1} + \frac{1}{n_2} \right)}} = 0.75$$

Verify($z_{3.5\text{mm}}$) = "reject alternative"

APPENDIX B: RELATIVE FLOW RATES

Analytic Viscosity: ν is viscosity in centistokes

$$f(x) := 49538 \cdot e^{-0.051 \cdot x}$$

$$cSt_{\text{water}} := .862 \quad cSt_{\text{gly}} := f(76) = 1027.101$$

$$w_{\text{water}} := .6 \quad w_{\text{gly}} := 1 - w_{\text{water}}$$

$$VBI_{\text{water}} := 14.534 \cdot \ln(\ln(cSt_{\text{water}} + .8)) + 10.975$$

$$VBI_{\text{gly}} := 14.534 \cdot \ln(\ln(cSt_{\text{gly}} + .8)) + 10.975$$

Mixture Equations

$$VBI_{\text{blend}} := w_{\text{water}} \cdot VBI_{\text{water}} + w_{\text{gly}} \cdot VBI_{\text{gly}}$$

$$\text{density} := (1260 \cdot w_{\text{gly}} + w_{\text{water}} \cdot 1000) \cdot \frac{\text{kg}}{\text{m}^3}$$

$$cSt_{\text{mix}} := \left(e^{\frac{VBI_{\text{blend}} - 10.975}{14.534}} - .8 \right) \cdot \frac{\text{mm}^2}{\text{s}}$$

$$cSt_{\text{mix}} = 0.000003443 \frac{\text{m}^2}{\text{s}}$$

$$\text{density} = 1104 \frac{\text{kg}}{\text{m}^3}$$

$$cP := 0.001 \text{ Pa} \cdot \text{s}$$

$$\mu_{\text{mix}} := cSt_{\text{mix}} \cdot \text{density}$$

$$\mu_{\text{mix}} = 0.0038 \text{ Pa} \cdot \text{s}$$

$$\mu_{\text{mix}} = 3.801 \text{ cP}$$

Original Values:

$$md_{aa} := 0.0175 \cdot \frac{\text{kg}}{\text{s}} \quad d_{aa} := 0.028 \text{ m} \quad A_{aa} := \frac{1}{4} \cdot \pi \cdot d_{aa}^2 \quad \rho := 1060 \cdot \frac{\text{kg}}{\text{m}^3}$$

$$md_{vad} := 0.053 \cdot \frac{\text{kg}}{\text{s}} \quad d_{vad} := 0.012 \text{ m} \quad A_{vad} := \frac{1}{4} \cdot \pi \cdot d_{vad}^2 \quad \mu := .004 \cdot \frac{\text{kg}}{\text{m} \cdot \text{s}}$$

$$V_{aa} := \frac{md_{aa}}{\rho \cdot A_{aa}} = 0.027 \frac{\text{m}}{\text{s}} \quad V_{vad} := \frac{md_{vad}}{\rho \cdot A_{vad}} = 0.442 \frac{\text{m}}{\text{s}}$$

$$Re_{aa} := \frac{\rho \cdot V_{aa} \cdot d_{aa}}{\mu} \quad Re_{vad} := \frac{\rho \cdot V_{vad} \cdot d_{vad}}{\mu}$$

$$Re_{aa} = 198.944$$

$$Re_{vad} = 1405.869$$

Mixture Values: Changed viscosity, need to decrease velocity to match Re

$$\mu_{\text{mix}} = 0.0038 \text{ Pa} \cdot \text{s}$$

$$V_{aa} := \frac{Re_{aa} \cdot \mu_{\text{mix}}}{\text{density} \cdot d_{aa}} = 0.02446 \frac{\text{m}}{\text{s}}$$

$$V_{vad} := \frac{Re_{vad} \cdot \mu_{\text{mix}}}{\text{density} \cdot d_{vad}} = 0.40338 \frac{\text{m}}{\text{s}}$$

$$md_{aa} := V_{aa} \cdot \text{density} \cdot A_{aa}$$

$$md_{vad} := V_{vad} \cdot \text{density} \cdot A_{vad}$$

$$md_{aa} = 0.01663 \frac{\text{kg}}{\text{s}}$$

$$md_{vad} = 0.050365 \frac{\text{kg}}{\text{s}}$$

$$\text{Vol_flow}_{aa} := A_{aa} \cdot V_{aa} \cdot \left[(100)^3 \cdot .001 \cdot 60 \right] \cdot \frac{s}{m^3} \quad \text{Vol_flow}_{vad} := V_{vad} \cdot A_{vad} \cdot \left[(10^2)^3 \cdot .001 \cdot 60 \right] \cdot \frac{s}{m^3}$$

conversion used:

$$\frac{m^3}{s} \cdot \frac{(100 \cdot \text{cm})^3}{1 \cdot m^3} \cdot \frac{.001 \cdot L}{1 \cdot \text{cm}^3} \cdot \frac{60 \cdot s}{1 \cdot \text{min}} = \frac{L}{\text{min}}$$

$$\text{Vol_flow}_{aa} = 0.90381 \quad \text{L/min}$$

$$\text{Vol_flow}_{vad} = 2.73725 \quad \text{L/min}$$

$$\text{Vol_flow}_{vad} + \text{Vol_flow}_{aa} = 3.641$$

Flow Rates:

$$\text{Sum} := \text{Vol_flow}_{aa} + \text{Vol_flow}_{vad} = 3.641$$

$$\text{DA} := \text{Sum} \cdot 0.61998 = 2.25738$$

$$\text{Ver} := \text{Sum} \cdot 0.046 = 0.16749$$

$$\text{Cora} := \text{Sum} \cdot 0.012 = 0.04369$$

$$\text{LCA} := \text{Sum} \cdot 0.08488 = 0.30905$$

$$\text{RCA} := \text{Sum} \cdot 0.08488 = 0.30905$$

$$\text{LSA} := \text{Sum} \cdot 0.0764 = 0.27818$$

$$\text{RSA} := \text{Sum} \cdot 0.0764 = 0.27818$$

$$\text{Sum_Out} := \text{DA} + \text{Ver} + \text{Cora} + \text{LCA} + \text{RCA} + \text{LSA} + \text{RSA} = 3.643$$

Volume Calculation

$$\rho_{\text{gly}} := 1.260 \frac{\text{gm}}{\text{cm}^3}$$

$$\rho_{\text{w}} := 1 \cdot \frac{\text{gm}}{\text{cm}^3}$$

graduated cylinder initial weight

$$W_0 := .15585 \cdot \text{kg}$$

cup weight

$$W_1 := .08141 \cdot \text{kg}$$

1 milliliter = 1 cubic centimeter

$$V_{\text{gly}} := 83\text{mL} \quad V_{\text{w}} := 417\text{mL} \quad V_{\text{max}} := 22\text{L}$$

Given

$$V_{\text{gly}} + V_{\text{w}} = V_{\text{max}}$$

$$\frac{V_{\text{gly}} \cdot \rho_{\text{gly}}}{V_{\text{w}} \cdot \rho_{\text{w}} + V_{\text{gly}} \cdot \rho_{\text{gly}}} = .4$$

$$\text{Volumes} := \text{Find}(V_{\text{gly}}, V_{\text{w}}) = \begin{pmatrix} 7.61246 \\ 14.38754 \end{pmatrix} \text{L}$$

$$V_{\text{gly}} := \text{Volumes}_0 = 7.612 \text{L}$$

$$V_{\text{w}} := \text{Volumes}_1 = 14.388 \text{L}$$

$$V_{\text{gly_gallon}} := V_{\text{gly}} \cdot \frac{.264172}{\text{L}} = 2.011$$

$$V_{\text{w_gallon}} := V_{\text{w}} \cdot \frac{.264172}{\text{L}} = 3.801$$

$$V_{\text{total_gal}} := V_{\text{gly_gallon}} + V_{\text{w_gallon}} = 5.812$$

$$V_{\text{total_L}} := V_{\text{gly}} + V_{\text{w}} = 22 \text{L}$$

$$W_{\text{gly}} := V_{\text{gly}} \cdot \rho_{\text{gly}} = 9.592 \text{kg} \quad W_{\text{w}} := V_{\text{w}} \cdot \rho_{\text{w}} = 14.388 \text{kg}$$

$$\frac{W_{\text{gly}}}{W_{\text{w}} + W_{\text{gly}}} = 0.4$$

$$\frac{W_{\text{w}}}{W_{\text{w}} + W_{\text{gly}}} = 0.6$$

$$W_{\text{total}} := V_{\text{gly}} \cdot \rho_{\text{gly}} + V_{\text{w}} \cdot \rho_{\text{w}} = 23.979 \text{kg}$$

$$\rho_{\text{mix}} := \frac{W_{\text{total}}}{V_{\text{max}}} = 1089.965 \frac{\text{kg}}{\text{m}^3}$$

for an 80/20 mixture,
measured SG was 1.05

REFERENCES

- ANSYS. "Fluent 6.3 User Guide." 2008.
- Argueta-Morales, IR, R Tran, W Clark, EA Divo, AJ Kassab, and WM Decampoli. "Surgical adjustment of the LVAD conduit to reduce thrombo-embolism: current results and progress towards multi-scale modeling." *Presented at First International Conference on Computational Simulation in Congenital Heart Disease (CS-CHD 2010)*, 2010.
- Argueta-Morales, IR, R Tran, W Clark, EA Divo, AJ Kassab, and WM DeCampoli. "Use of Computational Fluid Dynamics (CFD) to Tailor the Surgical Implantation of a Ventricular Assist Device (VAD): A Patient-Specific Approach to Reduce Risk of Stroke." *Journal of the American College of Surgeons*, 2010: S26.
- Bluestein, D, RT Schoepfoerster, and MK Dewanjee. "Steady flow in an aneurysm model: correlation between fluid dynamics and blood platelet deposition." *J Biomech Eng*, 1996: 280-286.
- Ceballos, A, AJ Kassab, R Osorio, EA Divo, IR Argueta-Morales, and WM Decampoli. "Computational Fluid Dynamics Analysis to Minimize Stroke Risk." *Faculty Podium Presentation by W. M. Decampoli at the The 3rd International Conference on Engineering Frontiers in Pediatric and Congenital Heart Disease*, May 2012.
- Davies, RR, et al. "The use of mechanical circulatory support as a bridge to transplantation in pediatric patients: an analysis of the United Network for Organ Sharing database." *JM.J Thorac Cardiovasc Surg.*, 2008: 421-427.
- DesJardins, S, et al. "'Tailoring' the Surgical Placement of Pediatric Ventricular Assist Devices (VAD) May Reduce Stroke Risk." *World Journal for Pediatric and Congenital Heart Surgery*, 2011: 187.
- Devore, JL. *Probability and statistics for engineering and sciences*. Brooks/Cole Publishing Co, 2004.
- Frazier, OH, and JK Kirklin. "Mechanical circulatory support, ISHLT Monograph." *Elsevier*, 2006: 1-8.
- Goldstein, DJ, MC Oz, and E Rose. "Implantable left ventricular assist devices." *N Engl J Med*, 1998: 2453-2456.
- John, R. "Current axial-flow devices--the HeartMate II and Jarvik 2000 left ventricular assist devices." *Semin Thorac Cardiovasc Surg*, 2008: 264-272.
- Laufer, G, et al. "First Clinical Experience With the DeBakey VAD Continuous-Axial-Flow Pump for Bridge to Transplantation." *Circulation*, 2000: 356-359.
- Layton, K, D Kallmes, H Cloft, E Lindell, and V Cox. "Bovine aortic arch variant in humans: clarification of a common misnomer." *Am J Neuroradiol*, 2006: 1541-1542.

- Lazar, RM, et al. "Neurological events during long-term mechanical circulatory support for heart failure: the randomized evaluation of mechanical assistance for the treatment of congestive heart failure (REMATCH) experience." *Circulation*, 2004: 2423-2427.
- Lietz, K, et al. "Impact of center volume on outcomes of left ventricular assist device implantation as destination therapy: analysis of the Thoratec HeartMate Registry, 1998 to 2005." *Circ. Heart Fail.*, 2009: 3-10.
- May-Newman, KD, BK Hillen, CS Sirona, and W Dembitsky. "Effect of LVAD outflow conduit insertion angle on flow through native aorta." *J Med Eng Technol*, 2004: 105-109.
- Menter, FR. "Two-equation eddy-viscosity turbulence models for engineering applications." *AIAA J*, 1994: 1598-1605.
- Meuris, B, J Arnout, D Vlasselaers, M Schetz, and B Meyns. "Long-term management of an implantable left ventricular assist device using low molecular weight heparin and antiplatelet therapy: a possible alternative to oral anticoagulants." *Artif Organs*, 2007: 402-405.
- Miller, LW, FD Pagani, SD Russell, and et al. "Use of a continuous-flow device in patients awaiting heart transplantation." *N Engl J Med*, 2007: 885-896.
- Nobili, M, J Sherrif, U Morbiducci, A Redaelli, and D Bluestein. "Platelet activation due to hemodynamic shear stresses: damage accumulation model and comparison to in vitro measurements." *Am Soc Artif Internal Organs J*, 2008: 64-72.
- Osorio, AF, AJ Kassab, EA Divo, IR Argueta-Morales, and WM DeCampli. "Computational Fluid Dynamics Analysis of Surgical Adjustment of Ventricular Assist Device Implantation to Minimize Stroke Risk." November 2009.
- Osorio, AF, Osorio, R., Tran. R., Ceballos, A., Kassab, A.J, Divo, E., Argueta-Morales, R., and DeCampli, W. "CFD Case Study to Optimize Surgical Adjustment of Ventricular Assist Device Implantation to Minimize Stroke Risk. Part I: Steady-State CFD Modeling." : *International Conference on Computational & Experimental Engineering and Sciences*. Las Vegas, April 1, 2010.
- Osorio, AF, Osorio, R., Ceballos, A., Tran, R., Clark, W., Divo, E.A., Argueta-Morales., I.R., Kassab, A.J., and DeCampli, W.M. "Computational Fluid Dynamics Analysis of Surgical Adjustment of Left Ventricular Assist Device Implantation to Minimize Stroke Risk." *Computer Methods in Biomechanics and Biomedical Engineering*, 2011.
- Pagani, FD, et al. "Extended Mechanical Circulatory Support With a Continuous-Flow Rotary Left Ventricular Assist Device." *Journal of the American College of Cardiology*, 2009.

- Pal, JD, et al. "Impact of left ventricular assist device bridging on posttransplant outcomes." *Ann Thorac Surg*, 2009: 1457-1461.
- Radovancevic, B, B Vrtovec, E de Kort, and et al. "End-organ function in patients on long- term circulatory support with continuous- or pulsatile-flow assist devices." *J Heart Lung Transplant*, 2007: 815-818.
- Radovancevic, R, et al. "Increased leukocyte-platelet interactions during circulatory support with left ventricular assist devices." *ASAIO J*, 2009: 459-464.
- Russo, MJ, et al. "Posttransplant survival is not diminished in heart transplant recipients bridged with implantable left ventricular assist devices." *J Thorac Cardiovasc Surg*, 2009: 1425-1432.
- Sandner, SE, et al. "Low molecular weight heparin as an alternative to unfractionated heparin in the immediate postoperative period after left ventricular assist device implantation." *Artif Organs*, 2008: 819-822.
- Schmid, C, et al. "Cerebral and systemic embolization during left ventricular support with the Novacor N100 device." *Ann Thorac Surg*, 1998: 1703-1710.
- Slater, JP, et al. "Low thromboembolic risk without anticoagulation using advanced-design left ventricular assist devices." *Circulation*, 1995: 467-471.
- Slaughter, MS, et al. "Advanced heart failure treated with continuous-flow left ventricular assist device." *N Engl J Med*, 2009: 2241-2251.
- Thoennissen, NH, et al. "Influence of inflammation and pump dynamic on cerebral microembolization in patients with Continuous-Flow DeBakey LVAD." *ASAIO J*, 2006: 243-247.
- Tsukui, H, et al. "Cerebrovascular accidents in patients with a ventricular assist device." *J Thorac Cardiovasc Surg*, 2007: 114-123.
- Waite, L, and JF Fine. *Applied biofluid mechanics*. New York: McGraw Hill Book Co., 2007.
- Wilcox, DC. *Turbulence modeling for CFD*. La Canada, CA: DCW Industries, Inc, 2006.